Marine and terrestrial climate variability in the western Mediterranean Sea during marine isotope stages 20 and 19

Francesco Toti, Adele Bertini, Angela Girone, Maria Marino, Patrizia Maiorano, Franck Bassinot, Nathalie Combourieu-Nebout, Sébastien Nomade, Antonella Buccianti

Marine and terrestrial climate variability in the western Mediterranean Sea during marine isotope stages 20 and 19

Francesco Toti[a], Adele Bertini[a, *], Angela Girone[b], Maria Marino[b], Patrizia Maiorano[b], Franck Bassinot[c], Nathalie Combourieu-Nebout[d], Sebastien Nomade[c], Antonella Buccianti[a]

[a]Dipartimento di Scienze della Terra, Università degli Studi di Firenze, via G. La Pira 4, 50121 Firenze, Italy

[b]Dipartimento di Scienze della Terra e Geoambientali, Università degli Studi di Bari Aldo Moro, via E. Orabona 4, 70125 Bari, Italy

[c]Laboratoire des Sciences du Climat et de l'Environnement UMR 8212, UVSQ, IPSL Université Paris Saclay, Gif-sur-Yvette, France

[d]HNHP UMR 7194 CNRS, Muséum National d'Histoire Naturelle, 1 rue René Panhard, 75013 Paris, France

Corresponding author. E-mail address: adele.bertini@unifi.it (A. Bertini).

Abstract

The climate variability within late Marine Isotope Stage (MIS) 20 and MIS 19 is examined with particular reference to the response of marine and terrestrial realms in the area surrounding the Alboran Sea (western Mediterranean Sea). Sediment samples from the Ocean Drilling Program Site 976 were used to derive high temporal resolution (average resolution of 450 years) palynological (pollen and spores) and calcareous plankton (coccolithophores and foraminifera) records. These data, together with the new $\delta^{18}O_{G.bulloides}$, make it possible to discuss the paleoenvironmental changes within a well constrained chronological frame. Cooler phases, including late MIS 20 and several cold spells during MIS 19b-a, are marked, on land, by the expansion of open vegetation formations dominated by steppe and semi-desert taxa. At the same time, the western Mediterranean Sea is marked by the incursion of North Atlantic polar-water planktonic taxa. MIS 19c and interstadials of MIS 19b-a are characterized by the spread of prevalent temperate forest taxa that parallel the expansion of warm-water calcareous plankton taxa during periods of lighter $\delta^{18}O$. Climate variations at both precessional and millennial to sub-millennial time-scales, expressed by on land and marine signals, highlight the sensitivity of the western Mediterranean area to both orbital forcing and rapid internal oscillations of the climate systems involving remote connections with North Hemisphere high latitudes.

The correlation within the central-western Mediterranean and North Atlantic climate dynamics including the time/spatial gradients related to regional and global climate processes contributes to the

reconstruction of the Earth climate dynamics and marine vs land responses, in full Early-Middle Pleistocene transition. These new evidences also provide an opportunity to improve knowledge of MIS 19c now considered, due to its orbital geometry, the best orbital analogue to the Holocene.

Keywords: MIS 19; Termination IX; Early-Middle Pleistocene Transition; western Mediterranean Sea; biotic proxies; stable isotopes; obliquity and precession forcing; millennial-scale climate variability; high to low-latitude forcing; land-sea correlations.

Highlights

1. High-resolution records document late MIS 20 and MIS 19 in western Mediterranean
2. Isotopes, calcareous plankton, pollen detect ocean temperature and vegetation changes
3. Land-ocean linkages are described over orbital and sub-millennial timescales
4. Tempo and Mode transition of Termination IX is traced
5. Intra-interglacial variability is evident by both marine and continental proxies

1. Introduction

During the whole Quaternary, glacial-interglacial cycles driven by quasi-periodical variations in the Earth's orbital parameters have repeatedly influenced the structure and dynamics of terrestrial and marine ecosystems. At the Early-Middle Pleistocene transition (EMPT; Head and Gibbard, 2015 and references therein), between 1.4 and 0.4 Ma, dominant cycles switched from 41 to 100 ka with progressively longer and colder glacials (e.g. Ruddiman et al., 1986; Maslin and Brierley, 2015). The onset of long-term glaciations left strong evidences in both marine and terrestrial biota, including extinctions and turnover phenomena (Head and Gibbard, 2015 and references therein). Millennial-scale oscillations lie superimposed over orbital-scale climate signals. Those recorded in high latitude sites were primarily associated with North Atlantic oceanic and atmospheric processes linked to ice-sheet dynamics (McAyeal, 1993; Marcott et al., 2011). In this context, recurring freshwater pulses explained the subpolar North Atlantic vertical convection and deep-water formation feeding the Atlantic Meridional Overturning Circulation (AMOC). More recently, especially by the study of Marine Isotope Stage (MIS) 19, millennial-scale climate oscillations have been related to highly nonlinear response to the Earth’s precession cycle and its harmonics (e.g. Ferretti et al., 2015; Sánchez Goñi et al., 2016; Oliveira et al., 2017; Nomade et al., 2019; Regattieri et al., 2019). The latter, which extended between 790-761 ka (Lisiecki and Raymo, 2005), is intensively studied because its warmest part (19c) is considered as the closest analogue of the current interglacial with

regards to astronomical and paleoclimatic signatures (Tzedakis et al., 2009, 2012a, b; Yin and Berger, 2012, 2015; Giaccio et al., 2015). The paleoclimatic and paleoceanographic records from extra-Atlantic sites, e.g. Osaka Bay (Hyodo et al., 2017) and Chiba (Suganuma et al., 2018) in Japan; Lake El'gygytgyn in far East Russia (Wennrich et al., 2014), Lake Baikal (Prokopenko et al., 2006) in southeastern Russia, and Antarctica (Jouzel et al., 2007), have also documented the occurrence of millennial-scale climate changes suggesting a global climatic teleconnection linked to North Atlantic ice-sheet dynamics during the MIS 20–19 transition (Termination IX: T-IX) and late MIS 19. In particular, the recent centennial-scale $\delta^{18}O$ records from the Chiba section throughout MIS 19 attest the influence of both North Atlantic climate variability, associated with AMOC disruption/reactivation due to freshwater discharges, and tropical insolation forcing on millennial-scale oceanographic variation and stability along the Kuroshio Extension Front (Haneda et al., 2020). The climate changes, related to the effects of both orbital and sub-orbital variations, that took place at global scale, are fully attested also in the Mediterranean Sea, an area highly sensitive to climate changes because, due to its mid-latitude position, it is strongly influenced by both polar and tropical dynamics (e.g. Lolis et al., 2002). In this area the millennial-scale climate oscillations, notably those throughout the latest MIS 20 and the entire MIS 19 (including MIS 19b-a) have been interpreted as strongly influenced by global climatic drivers and as the result of a strong teleconnection between atmospheric/sea surface-water conditions in the Mediterranean Sea, North Atlantic oceanic events and Northern Hemisphere ice sheet dynamics (Maiorano et al., 2016a; Nomade et al., 2019). Multiproxy records obtained on the Montalbano Jonico section (southern Italy) revealed the occurrence of a Heinrich-like event in late MIS 20 and warm-cold episodes (Bølling-Allerød-like and Younger-Dryas-like) during TIX (Maiorano et al., 2016a). The latter have been named terminal stadial Med-H_{TIX}, Med-BA_{TIX} and Med-YD_{TIX}, respectively in Marino et al., submitted), in analogy to those that occurred through the last termination (TI) (Maiorano et al., 2016a). For the eastern and central Mediterranean area the impact of climate changes on land is provided by several pollen-based vegetation records, at different resolution scale (e.g. Lake Ohrid, at the border between FYROM and Albania, Sadori et al., 2016, Wagner et al., 2019; Tenaghi Philippon, north-eastern Greece, Tzedakis et al., 2006; Tsampika, Rhodes, Greece, Joannin et al., 2007; Colfiorito, central Italy, Bertini, 2000; Montalbano Jonico section, southern Italy, e.g. Bertini et al., 2015), some of them focusing on MIS 19.

Finally, we would like to remind here that MIS 19 has also a particular, high stratigraphic relevance because it includes the Matuyama-Brunhes boundary, which was the primary guide for the Early-Middle Pleistocene boundary (Suganuma et al., 2018; Head, 2019 and references therein).

Here we present the results of a multi-proxy high-resolution quantitative study on calcareous plankton, palynomorphs and stables oxygen isotopes, carried out at Ocean Drilling Program (ODP) Site 976 from the Alboran Sea (Fig. 1). This key area is a gateway between the Mediterranean Sea and the Atlantic, and crossroads of polar and tropical systems, and provides a unique opportunity to document terrestrial and oceanic responses to global climate changes over the latest MIS 20 and MIS 19. The multi-proxy analyses, performed on the same samples, make it possible to reconstruct accurately the phase relationships between land-sea processes and climate impacts. A comparison of ODP site 976 with Atlantic (e.g. Site U1385 in southwestern Iberian, Sánchez Goñi et al., 2016) and central Mediterranean (e.g. Montalbano Jonico, Maiorano et al., 2016a; Nomade et al., 2019; Sulmona, Regattieri et al., 2019) sites provides new insights for the understanding of atmospheric and oceanic connections between these areas.

2. Regional setting

2.1. Geographic and depositional context

ODP Site 976 (36°12.3'N, 4°18.8'W) is located in the Alboran Sea (western Mediterranean Sea), ~110 km East of the Strait of Gibraltar, about 60 km and 150 km off the southern Spanish and northern Morocco coasts (Fig. 1). Drilling on this site, during ODP Leg 161 (Comas et al., 1996; Shipboard Scientific Party, 1996), allowed the recovery of a 346 m-long composite sedimentary succession. The record spans the uppermost Middle Miocene to the Holocene (Comas et al., 1996), providing important insights on both the depositional and palaeoceanographic history of the western Mediterranean Sea. Sedimentary cores mainly consist of nannofossil clays to silty-clays (Bernasconi et al., 1999) originating from pelagic sedimentation and turbidity flow mechanisms. The lithogenic fraction mostly comes from two sources: fluvial, supplied by the rivers draining the Betic Cordillera and southern Iberia coastal plains, and aeolian, which is linked to deflation processes from the nearby Sahara Desert (Fabres et al., 2002).

2.2. Oceanographic setting

Hydrodynamic in the Alboran Sea (Fig. 1) is governed by the Mediterranean thermohaline circulation system, which depends on the water exchange through the Strait of Gibraltar between the low salinity Atlantic surface inflow (Atlantic Jet: AJ; S=36.5 ‰) and the warm (13°C) high-salinity (38.4 ‰) (Candela, 2001) outflow from the Mediterranean Sea named, as it enters the Atlantic, Mediterranean Outflow Water (MOW). A permanent anti-estuarine circulation, maintained by the excess of evaporation within the Mediterranean Sea, drives the AJ to enter while the saltier MOW escapes at a deeper level. The AJ mixes with Mediterranean intermediate waters forming a 100-200 m thick layer,

the modified Atlantic water (MAW) that flows eastward (La Violette, 1994; Millot, 1999). The MOW results from the deeper, dense saline currents of the Levantine Intermediate Water (LIW) and Western Mediterranean Deep Water (WMDW) that flow westward, at deeper levels of the water column. LIW forms in the eastern Mediterranean Sea as a result of strong evaporation and sinking of the MAW (e.g. Millot, 1999). WMDW forms in the Gulf of Lion, and results from the winter cooling of surface waters by westerly winds (Millot, 1999). Two (prevalent) anticyclonic gyres, i.e. the Western (WAG) and Eastern Anticyclonic Gyre (EAG) are quasi- permanent features of the Alboran Sea circulation (Renault et al., 2012) generated by the MAW and westerly winds (Parrilla and Kinder, 1987) (Fig. 1). At the northern edges of the anticyclonic gyres, the AJ-MAW mixing produces a frontal system that favors vertical mixing and productive events, forming quasi-permanent areas of upwelling (García-Gorriz and Carr, 1999).

These hydro-climatic conditions affect the seasonal changes of the Alboran Sea's calcareous plankton assemblages. Species adapted to well-mixed and nutrient-rich sea surface water dominate during late fall and winter in coincidence with upwelling phenomena. Conversely, relaxed upwelling and/or stratified surface water conditions allow the proliferation of warm and oligotrophic planktonic taxa, mainly during summer and early fall (Barcena et al., 2004; Hernandez-Almeida et al., 2011).

2.3. Present climate and vegetation

The Alboran Sea area has a Mediterranean climate characterized by hot-dry summers and mild-humid winters (Walter et al., 1975; Quézel and Médail, 2003). Wintertime is subject to the arrival of Atlantic moist air masses (i.e. westerlies) whereas summertime is under the influence of the atmospheric subtropical high-pressure belt (Sumner et al., 2001). Sporadic but intense winds blow from the Sahara resulting from the northward shift of the Inter-Tropical Convergence Zone (ITCZ) (Guerzoni et al., 1997). Much of the present-day climate variability on a decadal to interannual time-scale has been linked to the North Atlantic Oscillation (NAO; Rodó et al., 1997), a meridional dipole of atmospheric pressure variability between Iceland and the Azores. In Europe NAO drives patterns and extremes in temperature, precipitation, snow cover and wind, especially during winter (Trigo et al., 2002; Comas-Bru and McDermott, 2014). Positive phases of NAO (NAO^+) usually correspond to warmer and wetter (colder and drier) winters in northern (southern) Europe; reverse patterns occur during negative phases (NAO^-).

Average annual precipitation along the nearby coasts of southern Spain varies from 300 mm to more than 1000 mm, with the highest values in the southwestern tips, which is the more exposed area to the rainfalls originating from the Atlantic storm-track and depressions (Sumner et al., 2001). A humid to sub-humid climate regime (600 to >800 mm/yr) is prevalent on the Northern Morocco coasts (Till

and Guiot, 1990). The vegetation of the Alboran borderlands complies with the general climate context though its distribution especially depends on both the maritime influence and presence of the Betic (Spain) and Rif (Morocco) mountains. The thermo to meso/supra altitudinal vegetation belts consist of thermophilic sclerophyllous scrublands (up to ~1200 m) underlying mixed evergreen/deciduous and deciduous oak forest at higher altitudes (~ 1200–1800 m; Rivas-Martínez, 1987). Coniferous taxa (with *Cedrus atlantica,* restricted to Morocco) requiring good soil-water availability expand on the mountain belt (Benabid, 1985; Nieto Caldera et al., 1990). *Pinus* spp. is a common component of both high-altitude and transitional woodlands (Benabid, 1982; Martinez Parras and Peinado Lorca, 1987). The highest altitudes (above ~ 2200 m) display juniper formations, shrublands of cushion-form xerophytes, and pasturelands. The driest areas (< 250 mm/yr) in both the lowland plains and high altitude plateaus display the development of steppe, either grass steppe dominated by *Stipa tenacissima*, or chamaephytic steppe dominated by *Artemisia herba-alba*.

3. Material and methods

The sedimentary section recovered at the ODP Site 976 was investigated for the interval 209.77-200.57 meters composite depth (mcd), that encompasses the late MIS 20 and MIS 19 intervals, according to the initial age model from de Kaenel et al. (1999) and Von Grafenstein et al. (1999). Sediment samples were obtained from the ODP Repository (Bremen). They were retrieved every 10 cm from holes B and C, and processed for planktonic foraminifera oxygen isotopic measurements, pollen and calcareous plankton analyses.

3.1 Stable isotopes measurement

Stable oxygen isotopes were measured on the planktonic foraminifer *Globigerina bulloides* (250-315 μm) in eighty-three samples. Analyses were performed on an Isoprime dual-inlet Isotope Ratio Mass Spectrometer (Elementar) at the Laboratory for Sciences of Climate and Environment (LSCE, France). Results are expressed as $\delta^{18}O$ vs V-PDB (in ‰). The external analytical reproducibility determined from replicate measurements of a carbonate standard is ± 0.05‰ (1σ). Values obtained for the calcite international standard NBS-18 for $\delta^{18}O$ is - 23.27‰. Measurements were usually performed using 4 to 15 individuals, except for five levels in which only 1 or 2 specimens of *G. bulloides* (e.g. 10 to 30 μg of $CaCO_3$) could be picked and analyzed. Measuring the isotopic composition of a large number of shells insures that potential heterogeneities in the foraminifer population (seasonality, bioturbation effects, ...) are smoothed out to some extent, providing a more robust result. Consequently, it is expected that isotopic data obtained on 1 or 2 shells could display a higher variability.

3.2. Calcareous plankton analysis

Calcareous plankton investigations were performed at the Department of Earth and Geoenvironmental Science, University of Bari Aldo Moro (Italy). Eighty-three samples were analyzed for planktonic foraminifera. The samples were dried and washed through 63 and 150 μm sieves. The residues (>150 μm) were split until a representative aliquot containing about 300 specimens had been obtained. All specimens were counted in the aliquots and species abundances were quantified as percentages on the total number of planktonic foraminifers.

Fifteen species or species groups were distinguished. The SPRUDTS group (sensu Rohling et al., 1993) includes *Trilobatus sacculifer*, *Hastigerina pelagica*, *Globoturborotalita rubescens*, *Orbulina universa*, *Beella digitata*, *Globoturborotalita tenella* and *Globigerinella siphonifera*. According to their ecological preference, the abundances of *Globigerinoides ruber* include *G. ruber* white and *Globigerinoides elongatus*. *G. ruber* and SPRUDTS group have been grouped as warm water taxa (Table I). For the taxonomy of *Neogloboquadrina* spp. the criteria from Darling et al. (2006) have been adopted: *Neogloboquadrina incompta* corresponds to what has been previously referred to *N. pachyderma* (dextral) and includes intergrades between *N. pachyderma* (dextral) and *N. dutertrei*; *N. pachyderma* only includes the left coiling specimens.

The investigation on calcareous nannofossil assemblages was performed on ninety-two samples. Slides for coccolithophore analysis were prepared according to the method of Flores and Sierro (1997) to estimate the absolute coccolith abundances (coccolith/g of sediment). Quantitative analyses were performed using a polarized light microscope at 1000X magnification and abundances were determined by counting at least 500 coccoliths of all sizes, in a varying number of fields of view. Reworked calcareous nannofossils (Cretaceous to Neogene in age) were estimated during this counting. Quantitative patterns of taxa were expressed as number of coccolith/g of sediment (N) and as percentages. *Umbilicosphaera* spp., *Calciosolenia* spp., *Oolithotus* spp., *Rhabdosphaera clavigera*, and *Discosphaera tubifera* were grouped as warm-water taxa (wwt), according to their ecological preferences (Table I). *Helicosphaera pavimentum*, which records a distinct positive relation with interglacial and interstadial phases, was also included in the wwt as already established in the Alboran Sea (Marino et al., 2018) and Balearic basin (Quivelli et al., 2020).

3.3. Palynological analysis

Ninety-three samples were processed for palynological analysis according to a standard procedure including HCl (at 18%) and HF (70%) digestion and a final filtration at 5 μm, at the Muséum National d'Histoire Naturelle (Paris). Tablets containing an aliquot number of exotic spores (*Lycopodium*)

were added to each sample, at the beginning of the preparation, to estimate the palynomorphs concentration. Residues were mounted in mobile slides, which were examined by transmitted-light optical microscope. Taxonomic identification conforms to reference collections and iconographic literature (e.g. Reille, 1992). Counts of at least 250 pollen grains, out of *Pinus*, were carried out on each sample to obtain quantitative estimation of taxa proportions. *Pinus* counts and percentage calculations were managed separately because of the large abundance of its pollen grains, a feature frequently observed in marine sediments and associated with overrepresentation phenomena (e.g. Heusser and Balsam, 1977). Counts of non-pollen palynomorphs including dinoflagellate cysts were carried out simultaneously, although only the frequency of *Isoetes* is shown here. Pollen taxa, except *Pinus*, are expressed in percentage normalized to a pollen sum without *Pinus*. *Pinus* relative abundance was calculated against the total pollen sum including its own grains. *Isoetes* was normalized to the total pollen plus *Isoetes* sum. In order to summarize the most significant changes of the palynological assemblages, selected taxa were also merged into informal groups on the base of the ecologic and climatic requirements of their present correspondents (Table II).

3.4 Statistical analysis

The statistical processing was first applied to a restricted set of variables (taxa or group of taxa, see Table III), which were a priori assumed to best summarize some ecological aspects. The data values were scaled by log-centered transformation to avoid biases linked to the compositional nature of the datasets (Aitchison, 1986; Aitchison and Greenacre, 2002). The management of count zero results would be preceded by a proper treatment of this type of data (Martín-Fernández et al., 2011). In our case the treatment of the 36 counts equal to zero involved a Bayesian inference related to a multinomial experiment and a multiplicative modification of the non-zero values in the vector of counts, knows as Bayesian-multiplicative (BM) treatment (Martín-Fernández et al., 2011; Martín-Fernández et al., 2015). The modification causes a minor distortion in the covariance structure and gives us an appropriate treatment to take into account the presence of zero values too (Martín-Fernández et al., 2012). Principal Component Analysis (PCA) was run to re-scale the original dataset variability to a lower- dimensional representation expressed by principal component axes. The main principal components of the three datasets were therefore reciprocally compared using a non-parametric correlation matrix to highlight possible correspondences along the succession. R-software different packages were used (R core Team 2019).

4. Results

4.1 Oxygen isotopes

The *G. bulloides* $\delta^{18}O$ data vary between ~0.50 and 2.63 ‰ (Fig. 2). From 209.27 mcd to 207.37 mcd, a decrease of nearly 1.8‰ of the $\delta^{18}O$ is observed, with values changing from ~2.4-2.6‰ to ~0.81‰ over the ~ 200 cm-thick interval. Upwards, the planktonic $\delta^{18}O$ record remains relatively constant, around ~0.7‰, with no clear oscillations up to 205.75 mcd (for a total thickness of 1.6 m). Then, the record shows a rapid change toward heavier $\delta^{18}O$, values increasing by ~0.7‰ in only 50 cm and reaching a maximum of 1.38‰ (Fig. 2). The upper portion of the record is characterized by several phases with low $\delta^{18}O$ values, limited by extremely abrupt $\delta^{18}O$ changes at their onsets and terminations. Two lighter episodes are visible in the $\delta^{18}O$ record over the intervals 204.95–203.67 mcd and 202.87–201.47 mcd. The low $\delta^{18}O$ values reached during the first climatic improvement (204.95-203.77 mcd) are slightly heavier than the values from the previous interval between 207.37 mcd and 205.75 mcd and show little variability. The beginning of the second climatic improvement interval (which ranges from 202.87-201.47 mcd) shows $\delta^{18}O$ values that are even lighter (peak value of ~ 0.5‰ at 202.67 mcd). The $\delta^{18}O$ values increase gradually upward to reach ~ 1.00 ‰ at 201.47 mcd, which corresponds to a change of ~0.5‰ in 1.2 m. This trend ends by a very rapid shift towards the second climatic degradation, with a change of ~1.4‰ in only 70 cm.

4.2 Calcareous plankton

Planktonic foraminifera are well preserved and diversified. The assemblages are mainly represented by *Neogloboquadrina* spp. (including *N. incompta*, *N. pachyderma* and *N. dutertrei*), *Turborotalita quinqueloba*, *G. inflata* and *G. bulloides* that are distributed through the entire section. *G. ruber*, SPRUDTS group and *Truncorotalia truncatulinoides* occur frequently from 208.8 mcd upward. Other less abundant taxa (subordinate taxa in Fig. 2) include *Globigerinita glutinata*, *Globorotalia scitula* and *Globigerina falconensis*, although never representing more than 16% of the total assemblage. *G. glutinata* occurs through the entire studied section, whereas *G. scitula* and *G. falconensis* have a more scattered distribution. Distribution patterns of abundance percentages of the main taxa allow identification of eight intervals (Ic to VIIIc) (Fig. 2). *G. inflata* and *G. bulloides*, representing about 70% of the total assemblages, are dominant taxa within Interval Ic. During the intervals IIc, IVc, VIc and VIIIc, *Neogloboquadrina* spp. and *T. quinqueloba* are the most abundant taxa representing from 50% up to 80% of the total assemblages. *Neogloboquadrina* spp. mainly consists of *N. pachyderma* in the intervals IIc, VIc and VIIc, while it is mainly made up of *N. incompta* and *N. dutertrei* during the other intervals. *G. ruber*, *G. inflata* and *G. bulloides* dominate the assemblages of the intervals IIIc, Vc and VIIc. During these intervals, SPRUDTS group and *Truncorotalia truncatulinoides* also became more abundant although never exceeding 12% of the assemblages.

Coccolithophore assemblages are generally well preserved, although some samples from the lower portion of the studied section show evidence of dissolution. Cretaceous to Paleogene reworked coccoliths have percentages lower than 2% with exception of the basal part of the record, where they reach up to 10-12 %. The total absolute abundance of coccolithophores varies from ca. 900 x 10^6 to 10000 x 10^6 coccolith/g of sediment with the higher values mainly in the interval 205.25-207.5 mcd. Thirty-two taxa have been recognized and they are mostly represented by gephyrocapsids that have abundance higher than 80-90 % (Fig. 2). Small gephyrocapsids (small *Gephyrocapsa* < 3 μ m) are dominant through the section and consist of morphotypes with closed (*G. caribbeanica*) and open central area, the latter including different taxa that were not distinguished at the species level (hereafter small *Gephyrocaspa* open central area). Gephyrocapsids larger than 3 μm are primarily *G. caribbeanica* and *G. oceanica*, with a minor percentage of *G. omega*. Other component of the assemblage is represented by less abundant taxa such as *Florisphaera profunda*, the wwt group, *Coccolithus* spp. (mainly *C. pelagicus* ssp. *pelagicus*), *Calcidiscus* spp. (mainly *C. leptoporus*), *Helicosphaera* spp. (mainly *H. carteri*), *Syracosphaera* spp. (*S. pulchra*, *S. hystrica*). Very rare and scattered occurrences of subordinate taxa are plotted as "other taxa" in Fig. 2 and they consist of *Pseudoemiliania lacunosa*, small *Reticulofenestra* spp., *Pontosphaera* spp., *R. clavigera* var. *stylifera*, *Braarudosphaera bigelowi*. Patterns of selected taxa are useful to distinguish eight intervals through the study record, in general agreement with the interval partition recognized by means of planktonic foraminifera (Ic to VIIIc). Small *G. caribbeanica* have their highest abundance during interval IIIc with an anti-covariant pattern in respect to other small gephyrocapsids. The wwt clearly show increase during the intervals IIIc-Vc, and VIIc, although a slight increase is also visible within interval I (Fig. 2). The most evident wwt decreases occur during intervals IIc, VIc and VIIIc and a short-term decrease may be observed within interval IVc. *Coccolithus* spp. distinctly increases up to 2% during intervals IIc and VIIIc (Fig. 2).

4.3 Palynomorphs

The rich and well-preserved palynoflora consist of 127 pollen taxa (28 arboreal and 99 non-arboreal) and 5 different morphotypes of Pteridophyta spores. Total pollen concentration ranges between 3000 and nearly 20 000 grains per gr of dry sediment (Fig. 3). *Pinus* concentration ranges between 410 and nearly 9200 grains per gr of dry sediment. Pollen assemblages mainly include taxa with a current wide distribution in (south) Europe and North Africa. Taxa, nowadays having an extra-Mediterranean distribution (such as *Carya* and *Tsuga*) or restricted in some geographical sectors of the Mediterranean area (such as *Liquidambar* and *Zelkova*), are subordinate. Deciduous oaks (*Quercus*) dominate the temperate broad-leaved forest assemblages whereas evergreen oaks and *Olea* are the

main components of the subordinate Mediterranean sclerophyll group. Among the high to mid altitude coniferous forest taxa *Cedrus* is especially abundant followed by *Abies* and *Picea*. Shrubs are mainly represented by Ericaceae and Cupressaceae followed by some Mediterranean taxa such as *Pistacia* and *Phillyrea*. Common herbaceous taxa include Asteraceae (mainly Cichorioideae), Poaceae, *Artemisia*, Amaranthaceae and *Ephedra* (Fig. 3) followed by Brassicaceae, *Plantago* and Cyperaceae. Among Pteridophyta the quillworts *Isoetes* is especially abundant. Throughout the palynological record eight informal intervals (Ip to VIIIp) have been established (Fig. 3). Temperate deciduous woody taxa plus Mediterranean sclerophyllous taxa are especially abundant (up to 56%) within IIIp, Vp and VIIp. A similar pattern is also recorded by *Isoetes*. Steppic and semi-desert taxa show the highest relative abundances (up to 52%) within Ip, IIp, IVp, VIp and VIIIp. The latter are often characterized, at their top, by some increase of mid to high altitudinal conifers such as *Cedrus* and *Abies*.

4.4 Statistical analysis

Simplified matrixes containing pollen, foraminifera and coccolithophores have been reconstructed (Table III). PCA performed on the matrix containing selected foraminifera taxa or ecological groups (Table I) revealed that two principal components, PC1-f and PC2-f, describe 87% of the total variance. The former is far more important, explaining 80 % of the total variance. Loadings of PC1-f are markedly positive for *G. ruber* group and SPRUDTS group while negative for *N. pachyderma* (Table III).

The simplified matrix containing the most significant calcareous nannofossil taxa or ecological groups reveals that 70 % of the variability are carried out by two principal components with PC1-n alone accounting for 48 % of the variance. PC1-n loads with positive score *C. pelagicus* spp. *pelagicus* and with negative scores warm water taxa, small *G. caribbeanica* and *G. caribbeanica* > 3μm (Table III).

For palynology the PCA shows that 87% of the variance of the pollen dataset variance can be expressed by two principal components (PC1-p and PC2-p). By investigating the behavior of the principal component axis, PC1-p (60 % of variability) in a binary plot result a high degree of anti-correlation can be observed. PC1-p has positive loadings for steppic and semi-desert taxa while has negative loadings for mesothermic broad-leaved and Mediterranean taxa (Table III).

4.5 Isotope stratigraphy and age model

The isotopic variations recorded by *G. bulloides* (Figs. 2-4) can be interpreted as a mix of surface water isotopic composition and temperature changes across the T.IX and over the MIS 19. MIS 19 starts above 207.67 mcd (Fig. 2) with a 1.9 m-thick deglaciation. It is a “step-like” deglaciation, with

a near-stabilization of the $\delta^{18}O$ values for ~70 cm, followed by a rapid change toward lighter values characteristic of full interglacial (MIS 19c hereafter). Starting at 207.35 mcd, the planktonic $\delta^{18}O$ values increase very slightly upward, showing no clear oscillations until 205.75 mcd (Fig. 2). Above 205.7 mcd, a rapid isotopic increase marks the end of MIS 19c and what we interpret as the beginning of MIS 19b. This increase in $\delta^{18}O$ corresponds to the first climatic degradation after the climatic optimum (interglacial *sensu-stricto*) as well as the beginning of millennial scale sub-orbital oscillations, which characterize the upper part of MIS 19 and which are well known in the Mediterranean realm (Giaccio et al., 2015; Sánchez Goñi et al., 2016; Simon et al., 2017; Nomade et al., 2019; Regattieri et al., 2019). The last part of MIS 19 shows three intervals with low $\delta^{18}O$ values (our record stops during the last of these low $\delta^{18}O$ intervals) suggesting returns to milder climatic conditions. These intervals are separated by returns to heavier $\delta^{18}O$ values with extremely abrupt onsets and terminations. During each successive climatic degradation, the average $\delta^{18}O$ values become heavier and closer to the values that are observed during the MIS 20 glacial. However, the $\delta^{18}O$ in MIS19b-a oscillations never reach a full glacial isotopic value suggesting that our Site 976 record does not reach the MIS 18 onset point (Figs. 2-4).

For many years, oxygen isotope chronostratigraphy had been based on the assumption that (i) benthic foraminifer $\delta^{18}O$ records chiefly contain a global isotopic signal associated with the waxing and waning of continental ice sheets, and that (ii) this signal was transferred within about ~ 1500 years across the world ocean along the *Great Conveyor Belt*. Over the recent years, however, it has become an evidence that benthic $\delta^{18}O$ records that are obtained in different oceanic basins or within different water masses may vary asynchronously across glacial-interglacial boundaries, with offsets up to several thousand years estimated for the last deglaciation for example (e.g. Skinner and Shackleton, 2005). It has been suggested that those spatial diachronisms are associated with reorganizations of ocean circulation patterns during the deglaciations. Such reorganizations result in asynchronous temperature changes in different areas of the world ocean, which superimpose on the ice volume signal (Waelbroeck et al., 2002; Skinner and Shackleton, 2005). Instead of using a unique $\delta^{18}O$ reference record to set chronostratigraphical frameworks in marine cores (e.g. LR04 from Lisiecki and Raymo, 2005), a recent work suggests that one should rather use reference records that are ocean- and depth-specific (Lisiecki and Stern, 2016). $\delta^{18}O$ diachronisms have been assessed by correlating the surface ocean hydrographic signals to nearby speleothem records whose chronologies rest upon independent, precise and accurate U/Th age models (Lisiecki and Stern, 2016).

A far as termination IX is concerned, there is no Mediterranean, reference isotopic record that properly accounts for a potential regional offset of foraminifer $\delta^{18}O$ relative to the global ice volume signal. Thus, in ODP 976, we dated the TIX $\delta^{18}O$ record using the same approach that was used for

the Montalbano section (Nomade et al., 2019). Assuming that TIX and MIS 19c are analogues to TI and the Holocene (Yin & Berger, 2012, 2015; Giaccio et al., 2015), we set the phasing of planktonic $\delta^{18}O$ changes relative to summer insolation across MIS20/MIS19 and early MIS19 to match the ^{14}C-dated phasing across the last termination (TI) (Martrat et al., 2014). The peak glacial of MIS 20 (heaviest *G. bulloides* $\delta^{18}O$ value) was set at ~ 797 ka, and the upper part of TIX was set at ~ 788 ka. The rapid oscillations that are clearly seen in ODP 976 planktonic record have been previously observed also in lacustrine records from central Italy (Giaccio et al., 2015; Regattieri et al., 2019) and high-resolution planktonic records from south Italy (Nomade et al., 2019) and the Iberian margin (Sanchez Goñi et al., 2016). A recent work suggested that these rapid oscillations likely reflect major disturbances of the hydrologic cycle associated with the ITCZ dynamics and/or to rapid disruptions in the transport of humidity by the westerlies (Nomade et al., 2019). Because these rapid oscillations involve atmospheric circulation, they should be synchronous over the whole Mediterranean area. Thus, the upper part of $\delta^{18}O$ oscillations in ODP 976 have been synchronized with those recorded in the Montalbano Ionico record (Nomade et al., 2019). The *G. bulloides* $\delta^{18}O$ record from ODP 976 is compared in figure 4 with the Montalbano Ionico record (Nomade et al., 2019) as well as with the IODP U1385 record from the Portuguese margin (Sánchez Goñi et al., 2016). This comparison shows that full interglacial conditions last longer on the Iberian Margin record, whereas the onset of MIS19b is found as early as 774 ka in the two Mediterranean isotopic records. This first marked increase in $\delta^{18}O$ takes place during a period of low boreal summer insolation (Fig. 4).
When applying our age model, the average time-resolution of ODP 976 $\delta^{18}O$ record is better than 400 years.

5. Discussion

5.1 Effects of climate changes on terrestrial and marine ecosystems

Quantitative analyses of calcareous plankton taxa and terrestrial palynomorphs (Figs. 2 and 3) provide evidence for variations of the surface and subsurface water parameters as well as for climate-related floristic and vegetational changes on land between about 801 and 760 ka (Table IV). Pollen data also contribute to reconstruct the tempo and mode in the reduction/disappearance phenomena of pollen taxa such as “Taxodiaceae”, *Cathaya* (plus *P. haploxylon* type), *Tsuga*, *Cedrus*, *Carya* and *Pterocarya* in the Mediterranean area. They suffered major progressive and diachronous reductions/disappearances under the effects of G/I cycles since the Gelasian as well as the drop in temperature and the change in the dominant cyclicity occurred during the Middle Pleistocene (e.g. Svenning, 2003; Bertini, 2010; Joannin et al., 2011; Magri and Palombo, 2013; Combourieu-Nebout et al., 2015; Magri et al., 2017). The identification of climatic gradients (under the effects of latitudes,

altitudes, and physiographies in the different sites) and the exact definition of a differentiated calendar of extinctions are both crucial to establish reliable correlations within marine and terrestrial sites of the Mediterranean area. At the ODP 976 the accurate stratigraphic distribution of taxa attests that the taxa mentioned above were already depleted but still present even if in very low quantities and discontinuously.

Main patterns of calcareous plankton assemblages in association with the PC1-f and PC1-n reveal that the abundance and distribution of foraminifera and coccolithophore taxa reflect changes in surface water temperature (Tables I, III, Figs. 2, 5). Positive score values, related to oligotrophic and tropical-subtropical warm-water *G. ruber* (Table I) highlight the occurrence of temperate-subtropical water conditions in the basin during the interglacial and interstadial phases. Negative values correspond to intervals with subpolar-transitional surface water conditions characterized by high abundances of *N. pachyderma*, a reliable indicator of polar/subpolar-water inflow in the Mediterranean basin during the Quaternary (Sierro et al., 2005; Girone et al., 2013a-b; Capotondi et al., 2016; Maiorano et al., 2016a, b; Bazzicalupo et al., 2018; Marino et al., 2018). The pattern of PC1-f describes eight intervals (Fig. 5) that are in good agreement with the distribution patterns of the investigated taxa (Fig. 2). Highest negative values are recorded during the MIS 20 glacial (interval IIc, Fig. 5) and during the stadials (intervals VIc and VIIIc, Fig. 5), suggesting more severe surface water cooling.

The PC1-n indicates an inverse relationship between subarctic *C. pelagicus* ssp. *pelagicus* (positive loading) and small *G. caribbeanica* together with wwt and *G. caribbeanica* > 3μm (negative loadings). The negative scores of PC1-n indicate the arrival of warmer and oligotrophic waters at the basin during the interglacial MIS 19c (interval IIIc in Figs. 2, 5) and the interstadials (intervals Vc and VIIc in Figs. 2, 5) while positive values indicate polar/subpolar water influx during late MIS 20 (interval IIc in Figs. 2, 5; Table I), MIS 19b and younger stadials, based on the ecological preferences of *C. pelagicus* ssp *pelagicus* and warm water taxa. The negative loadings of total *G. caribbeanica* suggest a preference for oligotrophic and warm surface waters at the study site, in agreement with Bollmann (1997) and Bollmann et al. (1998). The opposite loading (Table III) and anti-covariant patterns between total *G. caribbeanica* and small *Gephyrocapsa* with open central area (Fig. 2), the latter considered indicative of high productivity and unstable surface waters (Gartner et al., 1987; Gartner, 1988; Marino et al., 2008, 2011, 2018), is consistent with such interpretation and recent findings in the modern Alboran Sea, where the small *Gephyrocapsa* group (with open central area) positively responds to high nutrient content (Barcena et al., 2004; Ausin et al., 2015a, b).

Terrestrial counterpart of MIS 19c and successive interstadials are well represented by prevalent arboreal mesophilic vegetation typical of a (warm) temperate and relatively humid climate, according to pollen

evidence (IIIp, Vp, VIIIp; Figs. 3, 5; Table II). Deciduous trees, especially *Quercus* species, dominate this forest phase. Conversely, wooded steppes to steppes expanded during MIS 20 and successive stadials (IIp, IVp, VIp, VIIIp; Fig. 3) when cold and dry conditions prevailed. Such fluctuations show a strict correspondence with those expressed by the PC1-p values (Table III) (Fig. 5). PC1-p fluctuations allow the discrimination among plant communities with different thermal and humidity requirements (e.g. broad-leaved deciduous forest taxa, at - 0.48 vs steppic and semi-desert taxa, at 0.73). The PC1-p, PC1-f and PC1-n plots support the subdivision in both the eight informal calcareous plankton (Fig. 2) and pollen (Fig. 3) intervals whose time-boundaries even show a strict synchronicity (Fig. 5); so, by now, they will be identified in the text as common I-VIII merged phases (*MP*) for both marine and terrestrial biological proxies (Fig. 6). The correspondence revealed that temperate/subtropical surface water conditions were most probably synchronous with warm and wet climate conditions on land. Colder and harsher climate conditions on land occurred during the periods of prevailing subpolar/transitional surface–water conditions.

5.2 A coupled sea-land response during the latest MIS 20

The upward evolution from the base of the studied interval, between ca 801 and 800 ka (MP I in Fig. 6) is characterized by the progressive reduction in the atmospheric moisture amount, as attested by both the decreasing trend of Ericaceae, over about 1 ka long period, and the occurrence of herbs including steppic and semi-desert taxa (Fig. 6G) such as *Artemisia*, Amaranthaceae and *Ephedra* (Fig. 3, Table II), indicative of open vegetal formations under a prevalent (cold)-dry climate. In the sea, the parallel occurrence of *G. inflata* and *G. bulloides* (Fig. 6I), concomitant with very low percentages of warm and oligotrophic taxa in the calcareous plankton assemblages (Fig. 6C, E), document persistent cool, mixed and meso- to eutrophic sea surface water conditions. Within the same interval, the co-occurrence of subpolar *N. incompta* (Fig. 6B) and subarctic *C. pelagicus* ssp. *pelagicus* (Fig. 6D), although in very low abundances, also supports the hypothesis of cold sea surface waters.

Around 799 ka an impressive increase of *Artemisia*, *Ephedra* and Amaranthaceae (Fig. 6G plus Table II) along with the incoming decline of Ericaceae (Figs. 3, 6L) marks the major expansion of steppes and coastal salt marshlands in the Alboran Sea borderlands up to about 787 ka (MP II in Fig. 6). The notable harsher conditions on land parallel an abrupt expansion of polar-subpolar *N. pachyderma* and *C. pelagicus* ssp. *pelagicus* (Fig. 6B, D), suggesting a remarkable sea surface water temperature drop in the Alboran Sea and the onset of more severe glacial conditions. The colder seawater in the basin caused the decline of *G. inflata* in the basin (Fig. 6I) that proliferates in waters

with winter temperatures higher than 13°C as the modern Alboran Sea. The continued presence of polar-subpolar calcareous plankton taxa testifies that the coldest conditions persisted in sea surface waters up to 788 ka possibly linked to the arrival of polar-subpolar meltwater inflow into the basin from the Atlantic. Based on the abundance of key pollen and calcareous plankton taxa, we can identify three main sub-phases (IIa-c, Fig. 6). The first sub-phase (IIa) is marked by the strongest expansion of polar water taxa in the Alboran Sea (Fig. 6 B, D) and by the harshest conditions on land (Fig. 6G). The increase of the herbivorous species *T. quinqueloba* (Fig. 6J) suggests enhanced nutrient supply in the subsurface water masses and fresher surface water conditions (Rohling et al., 1997; Retailleau et al., 2012). *T. quinqueloba* abundance is high in areas with vigorous vertical mixing and nutrient-rich conditions (Reynolds and Thunell, 1986). Here its high abundance can result from a wind-induced mixing regime related to cold and arid climate conditions during an AMOC shutdown phase (Cacho et al., 2000; Moreno et al., 2004; 2005). During the sub-phase IIb, the increase of *N. incompta* at the expense of *N. pachyderma* (Fig. 6B) and the decline of *C. pelagicus* ssp. *pelagicus* (Fig. 6D) reflect the improvement of sea surface temperatures and the stronger stratification, since *N. incompta* prefers to dwell in a stratified mixed layer environment within the high-productivity zone associated with the development of a Deep Chlorophyll Maximum (DCM) (Fairbanks and Wiebe, 1980; Fairbanks et al., 1982; Rohling, 1997; Schiebel and Hemleben, 2005; Rigual-Hernandez et al., 2012). Despite the fact that the open vegetation is still dominant, the expansion of Cupressaceae (Fig. 6G) from about 795 ka likely reflects an increase of humidity on land. Many plants of Cupressaceae (e.g. *Juniperus, Tetraclinis*) have today, in the Alboran Sea land surroundings, a quite large altitude range, from sea level to high altitude, and can live in semiarid ombroclimatic zones as well as in humid ombroclimatic areas, such as some parts of Morocco and Algerian coasts (e.g. Quézel, 1980; Benabid, 1984). Their increase possibly reflects efficiency colonization under critical climate conditions associated with a strong reduction of warmer and humid demanding trees during TIX (sub-phase IIb), which also promoted low competitive pressure (McPherson and Wright, 1989). Under these climate conditions, even small increases in the amount of moisture in the air (e.g. fog and sea mist) could have favored the Cupressaceae expansion like it happens today for *Tetraclinis articulata* (Fennane et al., 1984). Such behavior seems attested by the oppositions between the Cupressaceae and steppic/semi-desertic percentage curves (Fig. 6G). Concurrent increases of *H. carteri* (Fig. 6F), likely as the result of the lower salinity and higher turbidity/detrital input in surface waters, are possibly linked to fresher Atlantic meltwater inflow and/or continental input related to a slight moisture improvement (Weaver and Pujol, 1988; Colmenero-Hidalgo et al., 2004; Hernández-Almeida et al., 2011; Maiorano et al., 2013, 2016b; Ausin et al., 2015a, b). The relative increase of moisture supply could be associated with a southward shift of mid-latitude westerly favored by southward

displacement of the thermal front and the development of strong mid-latitude meridional temperature gradient during reduction of AMOC and southward displacement of the ITCZ as previously suggested by Kageyama et al. (1999), Sepulchre et al. (2007), and Laîné et al. (2008). A similar scenario has been proposed to explain the increased wet conditions during H1 in the western Mediterranean, at both the ODP 976 site (Bazzicalupo et al., 2018) and the Iberian margin (Naughton et al., 2009). The slight increase of *G. bulloides* at this time (Fig. 6I) could also correspond to freshwater/terrigenous/nutrient input into the Alboran basin. According to some studies carried out across the Middle-Late Pleistocene terminations and TI (Sierro et al., 2005; Rogerson et al., 2008; Kandiano et al., 2012; Girone et al., 2013b; Bazzicalupo et al., 2018), local sources of freshwater could have arisen from melting of southern European and NW African (Atlas) mountain glaciers, playing an additional role in increasing river runoff. The large volume of freshwater deriving from Atlantic meltwater inflow via the Strait of Gibraltar and from on land local sources, could have depleted local seawater $\delta^{18}O$ culminating with a decrease up to 1.65‰ at 792 ka in coincidence with the major expansion of Cupressaceae. A similar, overall strong increase of Cupressaceae, centered at 790 ka, marks the latest MIS 20 at Montalbano Jonico (Maiorano et al., 2016a), located in the central Mediterranean. Such parallel occurrence in the Alboran and Ionian borderlands suggests a common mechanism in both areas, which might provide a regional stratigraphic marker at least at the Mediterranean scale, if not larger. During the same interval it is notable an increase of Cupressaceae, although at lower values. Moreover, this feature has been also recorded in the U1385 site from the Iberian margin (Sánchez Goñi et al., 2016).

The decrease of *N. pachyderma* and *C. pelagicus* ssp. *pelagicus*, between about 788 and 787 ka, indicates a reduction of polar water inflow into the Mediterranean during the transition MIS 20/MIS 19 at Site 976 (sub-phase IIc in Fig. 6). On land too, an overall progressive improvement of climate conditions is attested after the peak of steppic and semi-desert taxa around 788 ka. Within this interval, the increase of high to mid-altitude coniferous trees, notably *Cedrus* (Fig. 6H) parallels a slight increase of broad-leaved forest taxa (Fig. 6L), during intervening cool-humid conditions, possibly affecting prevalently upland areas. However, persistent overall, prevalent cold and dry conditions on land and reduced meltwater inflow could have resulted in increasing of column water ventilation favoring the advection of nutrient into the photic zone and the rising of pycnocline as suggested by the occurrence of *N. incompta* (Fig. 6B).

The arrival of polar sea water into the western Mediterranean Sea is coeval (within the uncertainties of respective age models) with pulses of cold and low salinity melt water masses, as revealed by low alkenone-SST and high $C_{37:4}$ peaks (Fig. 6R), during the terminal stadial at TIX in southwest Iberian margin (Site U1385, Rodrigues et al., 2017). Evidence of the incursion of polar water taxa associated

with the arrival of Atlantic meltwater masses at the central Mediterranean had been previously documented by Maiorano et al. (2016a) and Marino et al. (submitted), at Montalbano Jonico section (Ionian basin) where a terminal stadial, characterized by low alkenone-SST and increase in polar calcareous planktonic taxa, has been recognised at TIX as a regional equivalent of IRD discharge event (Heinrich-like event) in North Atlantic, related to millennial scale Northern Hemisphere ice-sheet collapse.

5.3 Marine and terrestrial evidence for millennia-scale climate oscillations during the earliest MIS 19

Short-term climate changes affected both land and sea environments (sub-phase MP IIIa in Fig. 6) with the first clear signal of ameliorated conditions just after 787 ka, in the earliest MIS 19c. On land, pollen assemblages indicative of cool and arid conditions show a clear, progressive reduction from 787 ka followed by a very short recovery of deciduous broad-leaved forest at 786 ka (Fig. 6L) suggesting a weak and short increase of temperature and humidity values. The strong increase of *G. inflata* (Fig. 6I) together with the gradual rising of all wwt in the planktonic foraminifera assemblages (Fig. 6C-E), although with low percentages, point to a warming in the surface waters and a restored deep pycnocline, between 787 and 785 ka. This warming phase may correspond to the northward migration of the polar front, as indicated by the disappearance of *N. pachyderma* (Fig. 6B) at the studied site and strongly reduced values of $C_{37:4}$ at Iberian margin (Fig. 6R), leading to the entrance of temperate-subtropical surface waters into the Alboran basin and the reactivation of AJ. The previous trend toward improved conditions is interrupted, around 785 ka, and marked by a prominent expansion of Asteraceae Cichorioideae (Fig. 6H) as well as a drastic decrease of *Pinus* (Fig. 3). At the same time *Isoetes*, a fern ally, strongly adapted to the seasonal flooding/desiccation pattern in ephemeral pools of the Mediterranean area (e.g. Medail et al., 1998; Keeley and Zedler, 1998; Molina, 2005), exhibits a marked step increase (Fig. 6K). Such climate reversal, during a weak summer insolation maximum, interrupts the warming climate of deglaciation possibly due to a change in seasonality during more continental climate conditions. The persistence of short warm summers (possibly quite dry) but with winter cooling (less dry) and short growing seasons could explain the major expansion of both Asteracee Cichoiroideae (without the recovering of steppe taxa) and *Isoetes* as well as the slight decrease of the deciduous broad-leaved forest. More severe winter conditions are also attested, among the foraminiferal assemblages, by the decline of *G. inflata* and the slight increase of *N. incompta*, at 784.8 ka (Hemleben et al., 1989; Pujol and Vergnaud-Grazzini, 1995; Schiebel et al., 2002; Rigual-Hernández et al., 2012). Increased winter wind-induced mixing promoted cooling of surface and subsurface waters, as suggested also by slight decrease of $PC1_{forams}$

and $PC1_{nanno}$ at this time (Fig. 5), and the advection of nutrients into the photic zone and the rising of pycnocline. The stratigraphical position of the Asteraceae event as well as its occurrence in coincidence of the first relevant *Isoetes* increase, just after a peak of deciduous broad-leaved forest at 786 ka recalls a similar event recorded in the Iberian record (Sánchez Goñi et al., 2016, here located at ca 787 ka) predating the onset of the terrestrial/Tajo interglacial in the earliest MIS 19c. Moreover, the same pattern of *Quercus* and Asteraceae pollen records has been recorded at Montalbano Jonico (i.e. event 1; Bertini et al., 2015) in the earliest MIS19c, concomitant with moderate cooling episode of the sea surface waters suggested by plankton assemblages (Maiorano et al., 2016a; Nomade et al., 2019). This event could correspond to the phase of reduced precipitation described by Regattieri et al. (2019) as event I, in the lacustrine sedimentary succession of Sulmona at 785 ka, despite the authors correlated it to the younger event 4 of Sánchez Goñi et al. (2016).

5.4 The full interglacial MIS 19c: timing and mode from land-sea comparison

Deciduous temperate taxa along with Mediterranean forest taxa exhibit a progressive expansion from 784.3 ka upwards supporting ameliorate climate conditions with increases of both temperature and humidity values. Those taxa plus *Isoetes* attest a new and progressive change in seasonality with higher winter precipitations and warmer and drier summers. Climate conditions on land are concurrent with a further increase in foram-wwt and increasing trend of total coccolith abundances. The $\delta^{18}O$ record also registers lighter values indicating the beginning of full interglacial conditions at about 783.5 ka although, solely since 782.2 ka, the full development of the mixed oak forest taxa, including the sclerophyllous scrubland ones, attests a net increase of both temperature and annual precipitation. This allows to draw a vegetation climate optimum on land lasting up to about 774 ka (Fig. 6L). The forest expansion, which lagged precession minima by ca 4/5 ka, suggests rather mild winter temperature and precipitation intensity that attest the effects of the westerlies controlled by the NAO (e.g. Gouveia et al., 2008; Wagner et al., 2019). However, four main contractions of the forest associated with slight increases of cosmopolitan herbaceous plants, more often Poaceae and Asteraceae, are centered at 781, 780, 777, and 775 ka, respectively. They suggest short-term climate changes inducing less humid conditions on land probably associated with a less humid winter season. In the sea, the coccolithophore assemblage likely benefited from less humid conditions as suggested by the increase of total coccolithophore abundances together with nanno-wwt (Fig. 6). Their behavior seems to be a positive ecological response to lower nutrient availability in the sea surface water. Still warm sea surface water conditions along with drought on land reduced the seasonal runoff leading to more year-round oligotrophy at the thermocline. Such short term events became more intense and more clearly expressed by humid/dry

fluctuations during the late MIS19c when the oscillations in temperate forest taxa were more pronounced and a slight expansion of steppic and semi-desert taxa has been observed along with a contraction of the Mediterranean taxa during insolation minima. During this time, it is likely that westerlies were slightly deflected toward the North with a subsequently reduced influence over the western Mediterranean area. At the Site U1385, in central southwestern Iberia, a dominant 5000-yr cyclicity of changes in the Mediterranean forest cover was associated with the response of the Earth system to the fourth harmonic of precession, which paced the shifting of the North Atlantic westerlies and the warm sea surface currents (Sánchez Goñi et al., 2016), and have been related to dry and cooler climate conditions. At Site 976 as well as at Site U1385, precession-driven climatic changes are well expressed in the distribution pattern of temperate deciduous forest taxa plus Mediterranean taxa to which millennial-scale events are superimposed. The four events of reduced humidity registered at ODP 976 fit very well with the repeated phases of reduced precipitations described at Sulmona in the same time interval (Regattieri et al., 2019) suggesting that at least the entire western Mediterranean area was affected by millennial drought events during MIS19c.

The distribution of Mediterranean pollen taxa and calcareous plankton species *G. caribbeanica* at Site 976 give additional insights concerning seasonal variations and plankton assemblage response to climate changes for this climatic interval. Mediterranean taxa abundance shows two main steps during the overall main phase of temperate deciduous forest taxa expansion. In the lower portion of MIS 19c the good expansion of Mediterranean taxa and *Isoetes* associated with a higher dry/humidity seasonal contrast during higher summer insolation. Later, during lower insolation (and a minimum of eccentricity), the reduction of Mediterranean taxa along with the weak expansion of Ericaceae induced lower rainfall seasonality but still at least 600 mm of annual precipitations as required by Ericaceae (Ozenda, 1982; Loidi et al., 2007). Between 782 and 778 ka (MP IIIb, Fig. 6), the maximum abundances of total *G. caribbeanica* (Fig. 6N) indicate more stable and oligotrophic conditions in the surface water. The co-occurrence in the foraminifera assemblages of *G. bulloides* and *G. inflata* (Fig. 6I) testifies the development of more nutrient content and ventilated conditions in the wintertime related to mild and humid conditions. The overall distribution pattern of calcareous plankton assemblages suggests the entrance of warmer and relatively nutrient-poor Atlantic water into the basin and the development of oceanographic conditions nearer to the modern ones, under a more Mediterranean climate regime as suggested by the pollen assemblages (general increase of pollen Mediterranean taxa). Anyway also total *G. caribbeanica* pattern shows short-term oscillations with highest abundances during relative less humid conditions suggesting more persistent oligotrophic sea surface conditions. The distinct occurrence of the tropical *T. sacculifer* (Fig. 6O) further supports persistent warm and oligotrophic surface water conditions, during less humid periods (Bé, 1977; Vincent and

Berger, 1981; Kucera et al., 2005; Munz et al., 2015; Capotondi et al., 2016; Maiorano et al., 2016b: Marino et al., 2018). This is consistent with the development of more prolonged summer hot and dry climate regime that affected the proliferation of *G. bulloides*. Later, from 778 ka upward, the higher abundances of the deep mixed dweller *T. truncatulinoides* (Fig. 6P) are interpreted as the result of enhanced seasonal mixing and eutrophic conditions related to more intense short-term dry and cooling events. At the studied site, the drop of *G. inflata* (Fig. 6I) and the higher abundances of small *Gephyrocapa* (with open central area) (Fig. 2) with respect to total *G. caribbeanica* (Fig. 2), during the late MIS19c, concurrent with the increasing of *N. incompta*, further support enhanced seasonal cooling, mixing and nutrient availability. Such environmental frame was likely favored by more intense wind-induced mixing during the development of seasonal climate regime toward cold and arid conditions, as suggested by the progressive increase of steppic taxa. The enduring occurrence of abundant foraminifera and coccolithophore warm water taxa (Fig. 6) and still high total coccolithophore production indicate that oceanographic conditions still allowed the seasonal formation of stratified, warm and oligotrophic conditions.

The direct comparison of marine and pollen proxies in the Alboran region supports a prevalent coupling in the air-sea response to climate during MIS 19c at both orbital and millennial time-scales.

5.5 Millennial scale climate variability through MIS 19b-a

A shift to colder and drier climate marked the onset of substages 19b-a (MP IV). On land a short-term cool-dry event, expressed by the expansion of steppe and semi-desert taxa (Fig. 6G), caused the partial opening of temperate deciduous forest and the contraction of thermophilous Mediterranean scrubland (Fig. 6L) with an acme centered around 773 ka.

Starting around 772 ka (from MPV upwards), the pollen record shows a high frequency variability expressed by the alternation between forested (MPV and MPVII) and open vegetation (MPVI and MPVIII) dominated phases corresponding to interstadial-stadial oscillations, respectively, in good agreement with the oscillations in the planktonic $\delta^{18}O$ curve in MIS 19b-a. They correlate with the coeval stadial-interstadial phases in the benthic $\delta^{18}O$ record in the Ionian Sea (Nomade et al., 2019). At Site 976, two first interstadial phases (Figs. 4, 6) are characterized by a progressive expansion of temperate-deciduous forest taxa with superimposed millennial to sub-millennial scale forest contractions and steppe increases (Fig. 6G, L). The overall percentage decrease of temperate deciduous taxa suggests the progressive decrease of annual precipitation and temperatures towards MPVII. Similar pattern is recorded in the Iberian margin site U1385 (see events 9-19 in Sánchez Goñi et al., 2016) and in the Sulmona basin (events VII to IX; Regattieri et al., 2019). At Site 976, in the sea, the interstadial (stadial) oscillations are evidenced by

the abundance fluctuations of warm (cold) water calcareous plankton taxa in good agreement with decrease (increase) of $\delta^{18}O$ (Fig. 5). These climate oscillations have been associated with cyclic northward shifts of ITCZ over the Mediterranean basin during a precession minimum (Nomade et al., 2019) in analogy with timing of the more recent wet periods that have occurred in the Mediterranean basin (e.g. Tzedakis, 2007; Milner et al., 2012; Regattieri et al., 2015). The northward position of ITCZ causes a northward shift of high-pressure system of the Mediterranean area, amplifying summer aridity in the region but in turn leading to enhanced winter precipitation. The increasing trends of *H. carteri* and *G. bulloides* during the interstadials concurrently with expansion of temperate-deciduous forest taxa and Mediterranean taxa suggest that the more humid conditions on land played an important role to feed the fluvial input leading to enhanced nutrient supply at sea surface waters. The northward shift of ITCZ was likely coupled by northward position of Azores Front and by the strength of Azores Current moving warm waters into the Mediterranean via Gibraltar Strait. The arrival of warm water at the basin favoured the proliferation of calcareous plankton wwt, and in particular foram-wwt that are characterised by abundance values very close to the percentages recorded during MIS19c. Ericaceae show peculiar phases of expansion and short-term fluctuations at the transition interstadial/stadial. This is especially evident in the latest portions of the two first interstadial oscillations of MIS19b-a when steppe plants start to increase and Mediterranean forest decrease. This vegetal assemblage, moving towards major cold and dry conditions, possibly supports the temporary occurrence of wet summers and prevalent drier winters during a cooler climate. In the sea, the coeval increase of *N. incompta* vs wwt in the late part of MIS19b-a interstadials could be considered as the response to these climate modifications. Cold and dry climate induced mixing and colder surface and subsurface sea water conditions, although we cannot exclude that this cooling was also related to both southward displacement of the Azores front and reduced northward transport of warm waters, probably linked to the gradual southward shift of subpolar front. In the nannofossil assemblages, the concomitant occurrence, although with very low abundances, of *C. pelagicus* ssp. *pelagicus* is a further support to this hypothesis. Such conditions together with those during previous warmer and moister interstadials promoted the instauration of thermal gradients and increase of the moisture availability arriving at northern latitudes contributing to the ice-growth. The significant expansion of steppic and semi-desertic taxa (MP VI and VIII; Fig. 6G) represents the vegetation response to the stadial climate, marked by drier conditions possibly responsible for the fall of *Isoetes* too. At the same time the sharp increases of polar-subpolar *N. pachyderma* and *T. quinqueloba* (Fig. 6B, J) suggest repeated inflow of fresher polar/subpolar waters into the Alboran Sea and drop in sea surface and subsurface temperatures. During the MPVI, the two prominent increases of the deep water dwelling *F. profunda* (Fig. 6Q), coincident with higher values in $\delta^{18}O$ (low salinity and cold surface

waters), could be interpreted as the result of short-term episodes of inverse thermocline, in agreement with previous Pleistocene very cold events in the Atlantic ocean (Colmenero-Hidalgo et al., 2004; Marino et al., 2014, 2018; Maiorano et al., 2015) and in Mediterranean Sea (Marino et al., 2018). The intrusion of colder and fresher meltwaters from Atlantic via Gibraltar Strait may have promoted enhanced stratification with cold surface waters and warmer subsurface waters at the thermocline/nutricline depth. The peaks of *F. profunda* are concurrent with relative decreases of the cold water taxa *N. pachyderma* and *N. incompta* supporting the hypothesis that ameliorated temperatures at the thermocline/nutricline depth, where they thrive, prevented their growth. Overall, the climate variability during MIS 19b-a, in the Alboran Sea, could also be the response to repeated shifts of westerlies, ITCZ and polar front relative position. Such scenario is coherent with the climate pattern recorded in other coeval Mediterranean sites (Nomade et al., 2019), in lacustrine sediments from central Italy (Giaccio et al., 2015; Regattieri et al., 2019) and with the climate patterns in North Atlantic (Channell et al., 2010; Kleiven et al., 2011; Tzedakis et al., 2012a, b; Emanuele et al., 2015; Ferretti et al., 2015; Sánchez Goñi et al., 2016), and Antarctic EDC ice core record (Jouzel et al., 2007; Pol et al., 2010).

6. Conclusion

The terrestrial (pollen) and marine (planktonic foraminifera and coccolithophores) records from ODP Site 976 document orbital and millennial scale climate fluctuations, during the latest MIS 20 and MIS 19, in the western Mediterranean area. The main abundance fluctuations of biological proxies match the planktonic $\delta^{18}O$ record describing MIS 19 stages and substages, and stadial-interstadial periods. The calcareous plankton and vegetation assemblage fluctuations are clearly in phase and evidence regional hydrological and atmospheric changes, which strongly interact with the complex ocean-atmosphere system.

The combined data-set allows the following deductions.

- During the latest phases of MIS 20 the western Mediterranean Sea was characterized by the instauration of cold sea surface temperatures and chiefly dry atmospheric conditions related to northern latitude ice-sheet dynamics, which induced the shutdown of the Atlantic Meridional Overturning Circulation (AMOC). Fluctuating pulses of polar water into the basin and alternations of cool-dry/cool-wetter climate conditions on land characterized the terminal stadial event, which occurred during the latest MIS 20.
- Since ca 787 ka, a progressive replacement of cold-climate vegetation by more thermophilous taxa and a progressive increase of warm-water taxa in calcareous assemblages mark the instauration of interglacial conditions in both terrestrial and marine realms.
- Climate optimum conditions were fully reached starting from about 782 ka up to about 774

ka, when a dominant temperate and humid climate on land and warm and stable sea surface waters established in the western Mediterranean.

- Superimposed to this general trend, short-term atmospheric and oceanographic changes characterized the MIS19.
- At about 785 ka, a significant increase of cosmopolitan herbs, notably Asteraceae, without major expansion of semi-desert vegetation, during an insolation maximum, marked a prominent climate change from warming to possibly quite (winter) cooler conditions and enhanced seasonality of precipitation. This event predates by about 3 ka, the climate optimum on land and it is correlated with the event 1 of the marine Montalbano Jonico section during the earliest MIS 19c in the central Mediterranean and with the event 1 in the lacustrine Sulmona basin in central Italy.
- During the ~ 10000 years that the MIS19c lasted, multiple forest declines mark short-term events of reductions of yearly humidity that could have affected the intensity of runoff and fluvial nutrient supply. Such conditions on land were coupled with more stable and oligotrophic conditions in the sea, as recorded by the increases of oligotrophic calcareous plankton key taxa.
- A first more prominent climate deterioration, centered around 773 ka, expressed by the instauration of atmospheric (cooler) drier conditions and cooler ocean surface waters, marks the beginning of MIS 19b-a.
- From around 773 ka upwards (MIS 19b-a), during one precession cycle, we observe two main high-amplitude millennial-scale oscillations in the calcareous plankton and pollen assemblages. These oscillations likely resulted from repeated shifts of westerlies, ITCZ and polar front relative position.
- The combined climate fluctuations as recorded by continental and marine proxies in Alboran Sea and the correlation with Iberian margin and Ionian Sea climate records confirm persistent oceanic and atmospheric interconnections between Mediterranean and North Atlantic climate regimes during latest MIS 20 and MIS 19.

Figure captions

Fig. 1. *A) Location of ODP Site 976 in the Alboran Sea (western Mediterranean), bathymetry of the area and modern-day oceanographic circulation: AJ (Atlantic Jet), MOW (Mediterranean Outflow Water), WMDW (Western Mediterranean Deep Water), LIW (Levantine Intermediate Water), MAW (Modified Atlantic Water), WAG (Western Alboran Gyre), EAG (Eastern Alboran Gyre). B) Location of IODP U1385, Sulmona and Montalbano Jonico (MJS) sites.*

Fig. 2. Cumulative abundances of planktonic foraminifera and coccolithophore assemblages plotted against the $\delta^{18}O$ vs depth. On the right the intervals discriminated according to the main calcareous plankton variation (see text for details).

Fig. 3. Selected palynological data expressed versus depth at ODP Site 976: Pollen concentration (grains/mL), (b); AP (Arboreal Pollen)/NAP (Non-Arboreal Pollen) percentage, (c); selected single and grouped pollen and spore taxa, (d). $\delta^{18}O$ record (a) is shown on the left and informal pollen zones (Ip-VIIIp) (e) on the right.

Fig. 4. Comparison of $\delta^{18}O$ record at the study site with the isotope records at the Montalbano Jonico section (Simon et al., 2017; Nomade et al., 2019) and North Atlantic IODP Site U1385 (Sánchez Goñi et al., 2016). Insolation curve from Laskar et al. (2004) is reported.

Fig. 5. First components obtained by Principal Component Analysis (PCA) performed on assemblages of planktonic foraminifera, coccolithophores and pollen at the study site, plotted against the $\delta^{18}O$ vs time. On the right the discriminated intervals discriminated based on the PCA on calcareous plankton (I-VIIIc) and pollen (I-VIIIp) assemblages.

Fig. 6. Abundance patterns of calcareous plankton and pollen key taxa (B-Q) plotted against $\delta^{18}O$ (A) vs time. On the right the Merged Phases (MP I-VIII) according to biotic proxies at the study site, and $C_{37:4}$ at the Site U1385 (Rodriguez et al., 2017). Obliquity, precession and insolation patterns are shown according to Laskar et al. (2004). Red arrows indicate temperate forest contractions and increase of total coccolithophore abundances. Black arrow indicates event 1 (Bertini et al., 2015).

TABLES
Tab. I – Summary of the main ecological preferences of calcareous plankton taxa according to several studies.
Tab. II – Informal pollen groups at ODP Site 976 with main floral components with their ecological significance and associated climate.
Tab. III – Loadings of selected pollen, foraminifera and calcareous plankton taxa or taxa groups on the first principal components at ODP Site 976. The most relevant component loadings are indicated in bold.
Tab. IV – Summary of the main paleoceanographic and paleoclimatic changes as recorded by calcareous plankton and pollen during the MIS 20–19 transition (Termination IX: T–IX) and late MIS 19 at the ODP Site 976 (Alboran Sea).TBl= temperate broad-leaved.

Acknowledgements

The authors thank the Ocean Drilling Program for providing the samples of ODP Site 976. The valuable suggestions and critical reviews from anonymous reviewers are greatly acknowledged. This research was financially supported by Università degli Studi di Firenze [Fondi di Ateneo A. Bertini 2013-15, and a Ph.D. fellowship to F. Toti]; Università degli Studi di Bari Aldo Moro [Fondi di Ateneo M. Marino] and benefited of instrumental upgrades from "Potenziamento Strutturale PONa3_00369 dell'Università degli Studi di Bari, Laboratorio per lo Sviluppo Integrato delle Scienze e delle Tecnologie dei Materiali Avanzati e per dispositivi innovativi (SISTEMA). The Authors thank the CNRS for financial support especially for pollen processes. This is LSCE contribution [n° 7051].

References

Aitchison, J., 1986. The statistical analysis of compositional data. Monographs on Statistics and Applied Probability, London, Chapman and hall Ltd, pp. 416.

Aitchison, J., Greenacre, M., 2002. Biplots of Compositional Data. Applied Statistics 51, 375–392.
Amore, F. O., Flores, J. A., Voelker, A. H. L., Lebreiro, S. M., Palumbo, E., Sierro, F. J., 2012. A Middle Pleistocene Northeast Atlantic coccolithophore record: Paleoclimatology and paleoproductivity aspects. Marine Micropaleontology 90–91, 44–59.
Ausín, B., Hernández-Almeida, I., Flores, J.-A., Sierro, F.J., Grosjean, M., Francés, G., Alonso, B., 2015a. Development of coccolithophore-based transfer functions in the western Mediterranean sea: a sea surface salinity reconstruction for the last 15.5 kyr. Climate of the Past 11, 1635–1651.
Ausín, B., Flores, J. A., Bácena, M. A., Sierro, F. J., Francés, G., Gutiérrez- Arnillas, E., Hernández-Almeida, I., Martrat, B., Grimalt, J. O., Cacho, I., 2015b. Coccolithophore productivity and surface water dynamics in the Alboran Sea during the last 25 kyr. Palaeogeogr. Palaeoclimatol. Palaeoecol. 418, 126–140.
Bárcena, M.A., Flores, J.A., Sierro, F.J., Perez-Folgado, M., Fabres, J., Calafat, A., Canals, M., 2004. Planktonic response to main oceanographic changes in the Alboran Sea (western Mediterranean) as documented in sediment traps and surface sediments. Marine Micropaleontology 53, 423– 445.
Bazzicalupo, P., Maiorano, P., Girone, A., Marino, M., Combourieu-Nebout, N., Incarbona, A. 2018. High-frequency climate fluctuations over the last deglaciation in the Alboran Sea, western Mediterranean: Evidence from calcareous plankton assemblages. Palaeogeogr. Palaeoclimatol. Palaeoecol. 506, 226–241.
Bé, A.W.H., 1977. An ecological, zoogeographic and taxonomic review of recent planktonic foraminifera. In: Ramsay, A.T.S. (Ed.) Oceanic Micropaleontology 1. Academic Press, London, p. 1.
Beaufort, L., Lancelot, Y., Camberin, P., Cayre, O., Vincent, E., Bassinot, F., Labeyrie, L., 1997. Insolation cycles as a major control of Equatorial Indian Ocean Primary Production. Science 278 1451–1454.
Beaufort, L., de Garidel-Thoron, T., Mix, A. C., Pisias, N. G., 2001. ENSO-like forcing on oceanic primary production during the late Pleistocene. Science 293, 2440–2444.
Benabid, A., 1982. Bref aperçu sur la zonation altitudinale de la végétation climacique du Maroc. Ecologia mediterranea 8.1/2, 301–315.
Benabid, A., 1984. Etude phytoécologique des peuplements forestiers et préforestiers du Rif centro-occidental (Maroc). Trav. Sci. Rabat, Sér. Bot. 34.
Benabid, A., 1985. Les écosystèmes forestiers et préforestiers du Maroc: diversité, répartition biogéographique et problèmes posés par leur aménagement. Forêt Méditerranéenne 7(1), 53–67.
Bernasconi, S.M., Meyers, P.A., O'Sullivan, G., 1999. Early diagenesis in rapidly accumulating sediments on the Alboran slope, ODP site 976. Geo-Marine Letters 18, 209–214.
Bertini, A., 2000. Pollen record from Colle Curti and Cesi: early and middle Pleistocene mammal sites in the Umbro-Marchean Apennine mountains (central Italy). J. Quat. Sci. 15(8), 825–840.
Bertini, A., 2010. Pliocene to Pleistocene palynoflora and vegetation in Italy: state of the art. Quat. Int. 225, 5–24. http://dx.doi.org/10.1016/j.quaint.2010.04.025.
Bertini, A., Toti, F., Marino, M., Ciaranfi, N., 2015. Vegetation and climate across the Early- Middle Pleistocene transition at the Montalbano Jonico section (southern Italy). Quat. Int. 383, 74–88.
Björck, S., Walker M. J. C., Cwynar, L. C., Johnsen, S., Knudsen, K-L., Lowe, J. J., Wohlfarth, B., INTIMATE Members, 1998. An event stratigraphy for the Last Termination in the North Atlantic region based on the Greenland Ice-core record: a proposal by the INTIMATE group. J. Quat. Sci. 13, 283–292.
Boeckel, B., Baumann, K.-H., 2004. Distribution of coccoliths in surface sediments of the south-eastern South Atlantic Ocean: ecology, preservation and carbonate contribution. Marine Micropaleontology 51 (3–4), 301–320.

Bollmann, J., 1997. Morphology and biogeography of *Gephyrocapsa* coccoliths in Holocene sediments. Marine Micropaleontology 29, 319–350.

Bollmann, J., Baumann, K.-H., Thierstein, H.R., 1998. Global dominance of *Gephyrocapsa* coccoliths in the late Pleistocene: selective dissolution, evolution, or global environmental change? Paleoceanography 13 (5), 517–529.

Cacho, I., Grimalt, J.O., Sierro, F.J., Shackleton, N., Canals, M., 2000. Evidence for enhanced Mediterranean thermohaline circulation during rapid climatic coolings. Earth Planet. Sci. Lett. 183 (3–4), 417–429.

Candela, J., 2001. Mediterranean water and global circulation. In Siedler, G., Church, J., and Gould, J., ed., Ocean Circulation and Climate: Observing and Modeling the Global Ocean: International Geophysics Series, v. 77: San Diego, California, Academic Press, 715 p.

Capotondi, L., Girone, A., Lirer, F., Bergami, C., Verducci, M., Vallefuoco, M., Afferri, A., Ferraro, L., Pelosi, N., De Lange, G.J., 2016. Central Mediterranean Mid-Pleistocene paleoclimatic variability and its connection with global climate. Palaeogeogr. Palaeoclimatol. Palaeoecol. 442, 72–83.

Channell, J.E.T., Hodell, D.A., Singer, B.S., Xuan, C., 2010. Reconciling astrochronological and 40Ar/39Ar ages for the Matuyama-Brunhes boundary in the late Matuyama Chron. Geochemical, Geophysical, Geosystem 11, Q0AA12. http://dx.doi.org/10.1029/2010GC003203.

Colmenero-Hidalgo, E., Flores, J.A., Sierro, F.J., Barcena, M.A., Lowemark, L., Schonfeld, J., Grimalt, J.O., 2004. Ocean surface water response to short-term climate changes revealed by coccolithophores from the Gulf of Cadiz (NE Atlantic) and Alboran Sea (W Mediterranean). Palaeogeogr. Palaeoclimatol. Palaeoecol. 205, 317–336.

Comas, M.C., Zahn, R., Klaus, A., et al., 1996. Proceeding of the Ocean Drilling Program, Initial Reports., 161, College Station, TX, 1023 pp.

Comas-Bru, L., McDermott, F., 2014. Impacts of the EA and SCA patterns on the European twentieth century NAO–winter climate relationship. Quarterly Journal of the Royal Meteorological Society 140(679), 354–363.

Combourieu-Nebout, N., Turon, J.-L., Zahn, R., Capotondi, L., Londeix, L., Pahnke, K., 2002. Enhanced aridity and atmospheric high-pressure stability over the western Mediterranean during the North Atlantic cold events of the past 50 ky. Geology 30, 863–866.

Combourieu-Nebout, N., Bertini, A., Russo-Ermolli, E., Peyron, O., Klotz, S., Montade, V., Fauquette, S., Allen, J., Fusco, F., Goring, S., Huntley, B., Joannin, S., Lebreton, V., Magri, D., Martinetto, E., Orain, R., Sadori, L., 2015. Climate changes in the central Mediterranean and Italian vegetation dynamics since the Pliocene. Rev. Palaeobot. Palynol. 218, 127–147. http://dx.doi.org/10.1016/j.revpalbo.2015.03.001.

Darling, K.F., Kucera, M., Kroon, D., Wade, C.M., 2006. A resolution for the coiling direction paradox in *Neogloboquadrina pachyderma*. Paleoceanography 21 (2), PA2011.

de Kaenel, E., Siesser, W. G., Murat, A., 1999. Pleistocene calcareous nannofossil biostratigraphy and the western Mediterranean sapropels, Sites 974 to 977 and 979. In Proceedings of the Ocean Drilling Program, scientific results (Vol. 161, pp. 159-183). College Station, Texas: Ocean Drilling Program.

Di Stefano, E., Incarbona, A., 2004. High resolution paleoenvironmental reconstruction of the ODP-963D Hole (Sicily Channel) during the last deglaciation, based on calcareous nannofossils. Marine Micropaleontology 52, 241–254.

Emanuele, D., Ferretti, P., Palumbo, E., Amore, F.O., 2015. Sea-surface dynamics and palaeoenvironmental changes in the North Atlantic Ocean (IODP Site U1313) during Marine Isotope Stage 19 inferred from coccolithophore assemblages. Palaeogeogr. Palaeoclimatol. Palaeoecol. 430, 104–117.

Fairbanks, R.G., Wiebe, P.H., 1980. Foraminifera and chlorophyll maximum: vertical distribution, seasonal succession, and paleoceanographic significance. Science 209 (4464), 1524–1526.

Fairbanks, R.G., Sverdlove, M., Free, R., Wiebe, P.H., Bé, A.W., 1982. Vertical distribution and isotopic fractionation of living planktonic foraminifera from the Panama Basin. Nature 298 (5877), 841.

Fabrés, J., Calafat, A., Sánchez-Vidal, A., Canals, M., Heussner, S., 2002. Composition and spatio-temporal variability of particle fluxes in the Western Alboran Gyre, Mediterranean Sea. Journal of Marine Systems 33, 431–456.

Fennane, M., Barbero, M., Quézel, P., 1984. Le thuya de Berbérie au Maroc: aperçu phytogéographique et écologique. Rabat, Bulletin de l'Institut Scientifique 8, 115–134.

Ferretti, P., Crowhurst, S.J., Naafs, B.D.A., Barbante, C., 2015. The Marine Isotope Stage 19 in the mid-latitude North Atlantic Ocean: astronomical signature and intra-interglacial variability. Quat. Sci. Rev. 108, 95–110.

Flores, J.A., Sierro, F.J., 1997. Revised technique for calculation of calcareous nannofossil accumulation rates. Micropaleontology 43, 321–324.

Ganopolski, A., Rahmstorf, S., 2001. Rapid Changes of glacial climate simulated in a coupled climate model. Nature 409, 153–158.

Garcia-Gorriz, E., Carr, M.E., 1999. The climatological annual cycle of satellite-derived phytoplankton pigments in the Alboran Sea. Geophys. Res. Lett. 26 (19), 2985–2988.

Gartner, S., 1988. Paleoceanography of the Mid-Pleistocene. Marine Micropaleontology 13, 23–46.

Gartner, S., Chow, J., Stanton, R.J.,1987. Late Neogene paleoceanography of the eastern Caribbean, the Gulf of Mexico, and the eastern Equatorial Pacific. Marine Micropaleontology 12 (3), 255–304.

Geisen, M., Billard, C., Broerse, A.T.C., Cros, L., Probert, I., Young, J.R., 2002. Life-cycle associations involving pairs of holococcolithophorid species: intraspecific variation or cryptic speciation? European Journal of Phycology 37, 531–550.

Geraga, M., Tsaila-Monopolis, S., Ioakim, C., Papatheodorou, G., Ferentinos, G., 2005. Short term climate changes in the southern Aegean Sea over the last 48,000 years. Palaeogeogr. Palaeoclimatol. Palaeoecol. 220, 311–332.

Giaccio, B., Regattieri, E., Zanchetta, G., Nomade, S., Renne, P.R., Sprain, C.J., Drysdale, R.N., Tzedakis, P.C., Messina, P., Scardia, G., Sposato, A., Bassinot, F., 2015. Duration and dynamics of the best orbital analogue to the present interglacial. Geology 43(7), 603–606.

Girone, A., Capotondi, L., Ciaranfi, N., Di Leo, P., Lirer, F., Maiorano, P., Marino, M., Pelosi, N., Pulice, I., 2013a. Paleoenvironmental change at the lower Pleistocene Montalbano Jonico section (southern Italy): global versus regional signals. Palaeogeogr. Palaeoclimatol. Palaeoecol. 371, 62–79.

Girone, A., Maiorano, P., Marino, M., Kucera, M., 2013b. Calcareous plankton response to orbital and millennial-scale climate changes across the Middle Pleistocene in the western Mediterranean. Palaeogeogr. Palaeoclimatol. Palaeoecol. 392, 105–116.

Gouveia, C., Trigo, R. M., DaCamara, C. C., Libonati, R., Pereira, J. M., 2008. The North Atlantic oscillation and European vegetation dynamics. International Journal of Climatology 28(14), 1835–1847.

Guerzoni, S., Molinaroli, E., Chester, R., 1997. Saharan dust inputs to the western Mediterranean Sea: depositional patterns, geochemistry and sedimentological implications. Deep-Sea Res. II 44, 631–645.

Haneda, Y., Okada, M., Kubota, Y., Suganuma, Y., 2020. Millennial-scale hydrographic changes in the northwestern Pacific during marine isotope stage 19: Teleconnections with ice melt in the North Atlantic. Earth Planet. Sci. Lett. 531, 115936.

Head, M. J., 2019. Formal subdivision of the Quaternary System/Period: Present status and future directions. Quaternary International, 500, 32–51.

Head, M.J., Gibbard, P.J., 2015. Early-Middle Pleistocene transitions: linking terrestrial and marine realms. Quat. Int. 389, 7–46.

Hemleben, C., Spindler, M., Anderson, O.R., 1989. Modern Planktonic Foraminifera. Springer-Verlag, New York (363 pp.).

Hernández-Almeida, I., Bárcena, M. A., Flores, J. A., Sierro, F. J., Sanchez- Vidal, A., Calafat, A.2011. Microplankton response to environmental conditions in the Alboran Sea (western Mediterranean): One year sediment trap record. Marine Micropaleontology 78, 14–24, 2011.

Heusser, L., Balsam, W. L., 1977. Pollen distribution in the northeast Pacific Ocean. Quat. Res. 7(1), 45–62.

Huber, R., Meggers, H., Baumann, K.-H., Raymo, M.E., Heinrich, R., 2000. Shell size variation of the planktonic foraminifer *Neogloboquadrina pachyderma* sin. in the Norwegian- Greenland Sea during the last 1.3 Myrs: implications for paleoceanographic reconstructions. Palaeogeogr. Palaeoclimatol. Palaeoecol. 160, 183–212.

Hyodo, M., Bradak, B., Okada, M., Katoh, S., Kitaba, I., Dettman, D.L., Hayashi, H., Kumazawa, K., Hirose, K., Kazaoka, O., Shikoku, K., Kitamura, A., 2017. Millennial-scale northern Hemisphere Atlantic-Pacifc climate teleconnections in the earliest Middle Pleistocene. Sci. Rep.7, 10036. https://doi.org /10 .1038 /s41598 -017 -10552 -2.

Joannin, S., Cornée, J.J., Moissette, P., Suc, J.-P., Koskeridou, E., Lécuyer, C., Buisine, C., Kouli, K., Ferry, S., 2007. Changes in vegetation and marine environments in the eastern Mediterranean (Rhodes Island, Greece) during the early and middle Pleistocene. Journal of Geological Society of London 164, 1119–1131.

Joannin, S., Bassinot, F., Combourieu-Nebout, N., Peyron, O., Beaudouin, C., 2011. Vegetation response to obliquity and precession forcing during the Mid-Pleistocene transition in western Mediterranean region (ODP site 976). Quat. Sci. Rev. 30, 280–297.

Jouzel, J., Masson-Delmotte, V., Cattani, O., Dreyfus, G., Falourd, S., Hoffmann, G., Minster, B., Nouet, J., Barnola, J. M., Chappellaz, J., Fischer, H., Gallet, J. C., Johnsen, S., Leuenberger, M., Loulergue, L., Luethi, D., Oerter, H., Parrenin, F., Raisbeck, G., Raynaud, D., Schilt, A., Schwander, J., Selmo, E., Souchez, R., Spahni, R., Stauffer, B., Steffensen, J. P., Stenni, B., Stocker, T. F., Tison, J. L., Werner, M., Wolff, E. W., 2007. Orbital and millennial Antarctic climate variability over the past 800,000 years. Science 317(5839), 793–796.

Kageyama, M., Valdes, P.J., Ramstein, G., Hewitt, C.D., Wyputta, U., 1999. Northern Hemisphere storm-tracks in present day and last glacial maximum climate simulations: a comparison of the European PMIP models. J. Climate 12, 742–760.

Kandiano, E.S., Bauch, H.A., Fahl, K., Helmke, J.P., Röhl, U., Pérez-Folgado, M., Cacho, I., 2012. The meridional temperature gradient in the eastern North Atlantic during MIS11 and its link to the ocean–atmosphere system. Palaeogeogr. Palaeoclimatol. Palaeoecol. 333–334, 24–39.

Keely, J.E., Zedler, P.H., 1998. Characterization and global distribution of vernal pools. In: Witham, C.W., Bauder, E.T., Belk, D., Ferren Jr., W.R., Ordunff, R. (Eds.). Ecology and management of vernal pool ecosystems. Proceedings from a 1996 Conference, California Native Plant Society, Sacramento, CA, USA, 1–14.

Kleiven, H., Hall, I.R., McCave, I.N., Knorr, G., Jansen, E., 2011. North Atlantic coupled deep-water flow and climate variability in the middle Pleistocene. Geology 39, 343–346.

Kucera, M., Kennett, J.P., 2002. Causes and consequences of a middle Pleistocene origin of the modern planktonic foraminifer *Neogloboquadrina pachyderma* sinistral. Geology 30, 539–542.

Kucera, M., Weinelt, M., Kiefer, T., Pflaumann, U., Hayes, A., Weinelt, M., Chen, M.-T., Mix, A.C., Barrows, T., Cortijo, E., Duprat, J., Juggins, S., Waelbroeck, C., 2005. Reconstruction of sea-surface temperatures from assemblages of planktonic foraminifera: multi- technique approach based on geographically constrained calibration datasets and its application to glacial Atlantic and Pacific Oceans. Quat. Sci. Rev. 24, 951–998.

Laîné, A., Kageyama, M., Salas-Mélia, D., Voldoire, A., Rivière, G., Ramstein, G., Planton, S., Tyteca, S., Peterschmitt, J.Y., 2008. Northern Hemisphere storm tracks during the Last Glacial Maximum in the PMIP2 ocean–atmosphere coupled models: energetic study, seasonal cycle, precipitation. Clim. Dyn. 32, 593–614.

Laskar, J., Robutel, P., Joutel, F., Gastineau, M., Correia, A.C.M, Levrard, B., 2004. Astrophysics A long-term numerical solution for the insolation. Astron. Astrophys. 285, 261–285.

La Violette, P.E., 1994. In: La Violette, P.E. (Ed.), Seasonal and Interannual Variability of the Western Mediterranean Sea, Coastal Estuarine Stud. vol. 46 AGU, Washington, D. C 373 pp.

Lisiecki, L. E., Raymo, M. E., 2005. A Pliocene-Pleistocene stack of 57 globally distributed benthic $\delta^{18}O$ records. Paleoceanography, 20(1).

Lisiecki, L. E., Stern, J. V., 2016. Regional and global benthic $\delta^{18}O$ stacks for the last glacial cycle. Paleoceanography, 31(10), 1368–1394.

Loidi, J., Biurrun, I., Campos, J. A., García-Mijangos, I., Herrera, M., 2007. A survey of heath vegetation of the Iberian Peninsula and Northern Morocco: a biogeographic and bioclimatic approach. Phytocoenologia, 37(3-4), 341–370.

Lolis, C.J., Bartzokas, A., Katsoulis, B.D., 2002. Spatial and temporal 850 hPa air temperature and sea-surface temperature covariances in the Mediterranean region and their connection to atmospheric circulation. Int. J. Climatol. 22, 663–676.

Magri, D., Palombo, M.R., 2013. Early to Middle Pleistocene dynamics of plant and mammal communities in south west Europe. Quat. Int. 288, 63–72. http://dx.doi.org/10.1016/j.quaint.2012.02.028.

Magri, D., Di Rita, F., Aranbarri, J., Fletcher, W., González-Sampériz, P., 2017. Quaternary disappearance of tree taxa from Southern Europe: Timing and trends. Quat. Sci. Rev., 163, 23–55.

Maiorano, P., Tarantino, F., Marino, M., De Lange, G.J., 2013. Paleoenvironmental conditions at Core KC01B (Ionian Sea) through MIS 13-9: evidence from calcareous nannofossil assemblages. Quat. Int. 288, 97–111.

Maiorano, P., Marino, M., Balestra, B., Flores, J.A., Hodell, D.A., Rodrigues, T., 2015. Coccolithophore variability from the Shackleton Site (IODP Site U1385) through MIS 16–10. Glob. Planet. Chang. 133, 35–48.

Maiorano, P., Bertini, A., Capolongo, D., Eramo, G., Gallicchio, S., Girone, A., Pinto, D., Toti, F., Ventruti, G., Marino, M., 2016a. Climate signatures through the Marine Isotope Stage 19 in the Montalbano Jonico section (Southern Italy): a land-sea perspective. Palaeogeogr. Palaeoclimat. Palaeoecol. 461, 341–361.

Maiorano, P., Girone, A., Marino, M., Kucera, M., Pelosi, N., 2016b. Sea surface water variability during the Mid-Brunhes inferred from calcareous plankton in the western Mediterranean (ODP Site 975). Palaeogeogr. Palaeoclimatol. Palaeoecol. 459, 229–248.

Marcott, S.A., Clark, P.U., Padman, L., Klinkhammer, G.P., Springer, S.R., Liu, Z., Otto-Bliesner, B.L., Carlson, A.E., Ungerer, A., Padman, J., He, F., Cheng, J., Schmittner, A., 2011. Ice-shelf collapse from subsurface warming as a trigger for Heinrich events. Proceedings of the National Academy of Sciences USA 108, 13415–13419.

Marino, M., Maiorano, P., Lirer, F., 2008. Changes in calcareous nannofossil assemblages during the Mid-Pleistocene Revolution. Marine Micropaleontology 69, 70–90.

Marino, M., Maiorano, P., Flower, B.P., 2011. Calcareous nannofossil changes during the Mid-Pleistocene revolution: paleoecologic and paleoceanographic evidence from North Atlantic Site 980/981. Palaeogeogr. Palaeoclimatol. Palaeoecol. 306(1–2), 58–69.

Marino, M., Maiorano, P., Tarantino, F., Voelker, A., Capotondi, L., Girone, A., Lirer, F., Flores, J.-A., Naafs, B.D.A., 2014. Coccolithophores as proxy of seawater changes at orbital- to-millennial scale during middle Pleistocene Marine Isotope Stages 14–9 in North Atlantic core MD01- 2446. Paleoceanography 29. PA002574.

Marino, M., Girone, A., Maiorano, P., Di Renzo, R., Piscitelli, A., Flores, J. A., 2018. Calcareous plankton and the mid-Brunhes climate variability in the Alboran Sea (ODP Site 977). Palaeogeogr. Palaeoclimatol. Palaeoecol. 508, 91-106.

Marino, M., Girone, A., Gallicchio, S., Herbert, T., Addante, M., Bazzicalupo, P., Quivelli, O., Bassinot, F., Bertini, B., Nomade, S., Ciaranfi, N., Maiorano, P. (2020). Climate variability

during MIS 20-18 as recorded by alkenone-SST and calcareous plankton in the Ionian Basin (central Mediterranean). Palaeogeogr. Palaeoclimatol. Palaeoecol. submitted.
Martín-Fernández, J.A., Hron, K, Templ, M., Filzmoser, P., Palarea-Albaladejo, J., 2012. Model-based replacement of rounded zeros in compositional data: Classical and robust approach. Computational Statistics & Data Analysis 56(3), 2688–2704.
Martín-Fernández, J.A., Hron, K., Templ, M., Filzmoser, P., Palarea- Albaladejo, J., 2015. Bayesian-multiplicative treatment of count zeros in compositional data sets. Statistical modeling 15(2), 134–158.
Martín-Fernández, J.A., Palarea-Albaladejo. J., Olea, R.A., 2011. Dealing with zeros, Ch. 4. In: Pawlowsky-Glahn V., Buccianti A. (Eds.). Compositional Data Analysis: Theory and Applications. Chichester, UK: John Wiley & Sons, Ltd, pp. 47–62.
Martinez Parras J.M., Peinado Lorca M., 1987. Andalucia oriental. In: Peinado Lorca M., Rivas Martinez S. (eds) La vegetacion de España. Universidad de Alcala de Henares, Alcala de Henares, Spain, pp 233–255.
Martrat, B., Jimenez-Amat, P., Zahn, R., Grimalt, J.O., 2014. Similarities and dissimilarities between the last two deglaciations and interglaciations in the North Atlantic region. Quat. Sci. Rev. 99, 122–134.
Maslin, M.A., Brierley, C.M., 2015. The role of orbital forcing in the Early Middle Pleistocene Transition. Quat. Int. 389, 47–55.
McAyeal, D.R., 1993. Binge/purge oscillations of the Laurentide ice sheet as a cause of North Atlantic's Heinrich events. Paleoceanography 8, 775–784.
McIntyre, A., Bè, A.H.W., 1967. Modern coccolithophores of the Atlantic Ocean - I. Placolith and cyrtoliths. Deep-Sea Research 14, 561–597.
McPherson, G.R., Wright, H.A., 1989. Direct effects of competition on individual juniper plants: a field study. Journal of Applied Ecology 26, 979–988.
Médail, F., Michaud, H., Molina, J., Paradis, G., Loisel, R., 1998. Conservation de la flore et de la végétation des mares temporaires dulçaquicoles et oligotrophes de France méditerranéenne. Ecologia Mediterranea 24, 119–134.
Millot, C., 1999. Circulation in the western Mediterranean Sea. Journal of Marine Systems 20, 423–442.
Milner, A.M., Collier, R.E.L., Roucoux, K.H., Müller, U.C., Pross, J., Kalaitzidis, S., Christanis, K., Tzedakis, P.C., 2012. Enhanced seasonality of precipitation in the Mediterranean during the early part of the Last Interglacial. Geology 40, 919-922.
Molfino, B., McIntyre, A., 1990a. Precessional forcing of nutricline dynamics in the equatorial Atlantic. Science 249, 766–769.
Molfino, B., McIntyre, A., 1990b. Nutricline variation in the equatorial Atlantic coincident with the Younger Dryas. Paleoceanography 5, 997–1008.
Molina, J.A., 2005. The vegetation of temporary ponds with *Isoetes* in the Iberian Peninsula. Phytocoenologia 35 (2-3), 219–230.
Moreno, A., Cacho, I., Canals, M., Grimalt, J.O., Sanchez-Vidal, A., 2004. Millennial-scale variability in the productivity signal from the Alboran Sea record, Western Mediterranean Sea. Palaeogeogr. Palaeoclimatol. Palaeoecol. 211 (3–4), 205–219.
Moreno, A., Cacho, I., Canals, M., Grimalt, J.O., Sánchez-Goñi, M.F., Shackleton, N., Sierro, F.J., 2005. Links between marine and atmospheric processes oscillating on a millennial time-scale. A multi-proxy study of the last 50,000 yr from the Alboran Sea (Western Mediterranean Sea). Quat. Sci. Rev. 24 (14–15), 1623–1636.
Munz, P.M., Siccha, M., Lückge, A., Böll, A., Kucera, M., Schulz, H., 2015. Decadal-resolution record of winter monsoon intensity over the last two millennia from planktic foraminiferal assemblages in the northeastern Arabian Sea. Holocene 25 (11), 1756–1771.

Naughton, F., Sánchez Goñi, M.F., Kageyama, M., Bard, E., Duprat, J., Cortijo, E., Desprat, S., Malaize, B., Joly, C., Rostek, F., Turon, J.L., 2009. Wet to dry climatic trend in northwestern Iberia within Heinrich events. Earth Planet. Sci. Lett. 284 (3–4), 329–342.

Nieto-Caldera, J.M., Pérez-Latorre, A.V., Cabezuto, B., 1990. Datos sobre la vegetacion silicicola de Andalucia. I. Acta Botánica Malacitana 15, 179–192.

Nomade, S., Bassinot, F., Marino, M., Simon, Q., Dewilde, F., Maiorano, P, Isguder, G., Blamart, D., Girone, A., Scao, V., Pereira, A., Toti, F., Bertini, A., Combourieu-Nebout, N., Peral, M., Bourlès, D.L., Petrosino, P., Gallicchio, S., Ciaranfi, N., 2019. High-resolution foraminifer stable isotope record of MIS 19 at Montalbano Jonico, southern Italy: A window into Mediterranean climatic variability during a low-eccentricity interglacial. Quat. Sci. Rev. 205, 106–125.

Oliveira, D., Sánchez Goñi, M. F. S., Naughton, F., Polanco-Martínez, J. M., Jimenez-Espejo, F. J., Grimalt, J. O., Martrat, B., Voelker, A.H.L., Trigo, R., Hodell, D., Abrantes, F., Abrantes, F., 2017. Unexpected weak seasonal climate in the western Mediterranean region during MIS 31, a high-insolation forced interglacial. Quat. Sci. Rev. 161, 1–17.

Ozenda, P., 1982. Plants in the biosphere. Ed. Doin, Paris, 427.

Palumbo, E., Flores, J.A., Perugia, C., Petrillo, Z., Voelker, A.H.L., Amore, F.O., 2013. Millennial scale coccolithophore paleoproductivity and surface water changes between 445 and 360 ka (Marine Isotope Stages 12/11) in the Northeast Atlantic. Palaeogeogr. Palaeoclimatol. Palaeoecol. 383–384, 27–41.

Parente, A., Cachão, M., Baumann, K.-H., de Abreu, L., Ferreira, J., 2004. Morphometry of *Coccolithus pelagicus* s.l. (Coccolithophore, Haptophyta) from offshore Portugal, during the last 200 kyr. Micropaleontology 50, 107–120.

Parrilla, G., Kinder, T.H., 1987. Oceanografia fisica del mar de Alboran. Boletin del Instituto Espanol de Oceanografia 4, 133– 165.

Prokopenko, A.A., Hinnov, L.A., Williams, D.F., Kuzmin, M.I., 2006. Orbital forcing of continental climate during the Pleistocene: a complete astronomically tunedcli-matic record from Lake Baikal, SE Siberia. Quat. Sci. Rev.25, 3431–3457. https://doi.org /10 .1016 /j .quascirev.2006 .10 .002.

Pujol, C., Vergnaud-Grazzini, C., 1995. Distribution patterns of live planktic foraminifers as related to regional hydrography and productive systems of the Mediterranean Sea. Marine Micropaleontology 25, 187–217.

Pol, K., Masson Delmotte, V., Johnsen, S., Bigler, M., Cattani, O., Durand, G., Falourd, S., Jouzel, J., Minster, B., Parrenin, F., Ritz, C., Steen Larsen, H.C., Stenni, B., 2010. New MIS 19 EPICA Dome C high resolution deuterium data: hints for a problematic preservation of climate variability at sub-millennial scale in the “oldest ice”. Earth Planet. Sci. Lett. 298, 95.103.

Quézel, P., 1980. Biogéographie et écologie des conifères sur le pourtour méditerranéen. In. Person. Actualité d’écologie forestière. Ed. Bordas, Paris., 205–256.

Quézel, P., Médail, F., 2003. Écologie et biogeographie des forêts du bassin méditerranéen. Elsevier, Paris, pp. 571.

Quivelli, O., Marino, M., Rodrigues, T., Girone, A., Maiorano, P., Abrantes, F., Salgueiro, E., Bassinot, F., 2020. Surface and deep water variability in the Western Mediterranean (ODP Site 975) during insolation cycle 74: High-resolution calcareous plankton and molecular biomarker signals. Palaeogeogr. Palaeoclimatol. Palaeoecol. 542, 109583. https://doi.org/10.1016/j.palaeo.2019.109583

R Core Team, 2019. R: A language and environment for statistical computing. R Foundation for Statistical Computing, Vienna, Austria. URL http://www.R-project.org/.

Regattieri, E., Giaccio, B., Zanchetta, G., Drysdale, R.S., Galli, P., Peronace, E., Nomade, S., Wulf, S., 2015. Hydrological variability over Apennine during the Early Last Glacial precession minimum, as revealed

by a stable isotope record from Sulmona basin, central Italy. J. Quat. Sci. 30, 19–31, doi:10.1002/jqs.2755.

Regattieri, E., Giaccio, B., Mannella, G., Zanchetta, G., Nomade, S., Tognarelli, A., Perchiazzi, H., Vogel, N., Boschi, C., Drysdale, R.N., Wagner, B., Gemelli, M., Tzedakis, P., 2019. Frequency and dynamics of millennial-scale variability during marine isotope stage 19: insights from the Sulmona Basin (central Italy). Quat. Sci. Rev. 214, 28–43

Reille, M., 1992. Pollen et spores d'Europe et d'Afrique du nord (Pollen and Spores of Europe and North Africa). Laboratoire de Botanique historique et Palynologie, Marseille.

Renault, L., Oguz, T., Pascual, A., Vizoso, G., Tintore, J., 2012. Surface circulation in the Alborán Sea (western Mediterranean) inferred from remotely sensed data. Journal of Geophysical Research 117, 1–11.

Retailleau, S., Eynaud, F., Mary, Y., Abdallah, V., Schiebel, R., Howa, H., 2012. Canyon heads and river plumes: how might they influence neritic planktonic foraminifera communities in SE Bay of Biscay? Journal of Foraminiferal Research 42 (3), 257–269.

Reynolds, L. A., Thunell, R. C., 1986. Seasonal production and morphologic variation of *Neogloboquadrina pachyderma* (Ehrenberg) in the northeast Pacific. Micropaleontology 32, 1–18.

Rigual-Hernández, A.S., Sierro, F.J., Bárcena, M.A., Flores, J.A., Heussner, S., 2012. Seasonal and interannual changes of planktic foraminiferal fluxes in the Gulf of Lions (NW Mediterranean) and their implications for paleoceanographic studies: two 12- year sediment trap records. Deep-Sea Res. I Oceanogr. Res. Pap. 66, 26–40.

Rivas-Martínez, S., 1987. Memoria del mapa de las series de vegetación de España. Icona, Madrid. 268 pp.

Rodó, X., Baert, E., Comin, F.A., 1997. Variations in seasonal rainfall in Southern Europe during the present century: relationships with the North Atlantic Oscillation and the El Niño-Southern Oscillation. Climate Dynamics 13, 275–284.

Rodrigues, T., Alonso-García, M., Hodell, D.A., Rufino, M., Naughton, F, Grimalt, J.O., Voelker, A.H.L., Abrantes, F., 2017. A 1-Ma record of sea surface temperature and extreme cooling events in the North Atlantic: A perspective from the Iberian Margin. Quat. Sci. Rev. 172, 118-130.

Rogerson, M., Cacho, I., Jimenez-Espejo, F., Reguera, M.I., Sierro, F.J., Martinez-Ruiz, F., Canals, M., 2008. A dynamic explanation for the origin of the western Mediterranean organic-rich layers. Geochem. Geophys. Geosyst. 9 (7).

Rohling, E.J., Jorissen, F.J., Vergnaud Grazzini, C., Zachariasse, W.J., 1993. Northern Levantine and Adriatic Quaternary planktic foraminifera; reconstruction of paleoenvironmental gradients. Mar. Micropaleontogy 21, 191–218.

Rohling, E.J., den Dulk, M., Pujol, C., Vergnaud-Grazzini, C., 1995. Abrupt hydrographic changes in the Alboran Sea (western Mediterranean) around 8000 yrs BP. Deep-Sea Res. 42, 1609–1619.

Rohling, E.J., Jorissen, F.J., De Stigter, H.C., 1997. 200 year interruption of Holocene sapropel formation in the Adriatic Sea. J. Micropalaeontol. 16 (2), 97–108.

Ruddiman, W. F., Raymo, M., McIntyre, A., 1986. Matuyama 41,000-year cycles: North Atlantic Ocean and northern hemisphere ice sheets. Earth Planet. Sci. Lett. 80, 117–129.

Saavedra-Pellitero, M., Flores, J.A., Baumann, K.-H., Sierro, F.J., 2010. Coccolith distribution patterns in surface sediments of Equatorial and Southeastern Pacific Ocean. Geobios 43, 131–149.

Sadori, L., Koutsodendris, A., Panagiotopoulos, K., Masi, A., Bertini, A., Combourieu-Nebout, N., Francke, A., Kouli, K., Joannin, S., Mercuri, A.M., Peyron, O., Torri, P., Wagner, B., Zanchetta, G., Sinopoli, G., Donders, T.H., 2016. Pollen-based paleoenvironmental and paleoclimatic change at Lake Ohrid (south-eastern Europe) during the past 500 ka. Biogeosciences 13, 1423–1437.

Sánchez Goñi, M.F., Rodrigues, T., Hodell, D.A., Polanco-Martínez, J.M., Alonso-García, M., Hernández-Almeida, I., Desprat, S., Ferretti, P., 2016. Tropically-driven climate shifts in

southwestern Europe during MIS 19, a low eccentricity interglacial. Earth Planet. Sci. Lett. 448, 81–93.

Schenk, F., Väliranta, M., Muschitiello, F., Tarasov, L., Heikkilä, M., Björck, S., Brandefelt, J., Johansson, A. V., Näslund, J.O., Wohlfarth, B., 2018. Warm summers during the Younger Dryas cold reversal. Nature communications 9.

Schiebel, R., Hemleben, C., 2005. Modern planktic foraminifera. Paläontologische Zeitschrift, 79 (1), 135–148

Schiebel, R., Waniek, J., Zeltner, A., Alves, M., 2002. Impact of the Azores Front on the distribution of planktic foraminifers, shelled gastropods, and coccolithophorids. Deep-Sea Res. Part 2 49, 4035–4050.

Sepulchre, P., Ramstein, G., Kageyama, M., Vanhaeren, M., Krinner, G., Sánchez Goñi, M.-F., d'Errico, F., 2007. H4 abrupt event and late Neanderthal Presence in Iberia. Earth Planet. Sci. Lett. 258, 283–292. doi:10.1016/j.epsl.2007.03.041

Shipboard Scientific Party, 1996. Site 976, Comas, M.C., Zahn, R., Klaus, A., et al., (Eds.), Proc. ODP Init. Repts., College Station, TX Vol. 161, 179–297.

Sierro, F.J., Hodell, D.A., Curtis, J.H., Flores, J.A., Reguera, I., Colmenero- Hidalgo, E., Bárcena, M.A., Grimalt, J.O., Cacho, I., Frigola, J., Canals, M., 2005. Impact of iceberg melting on Mediterranean thermohaline circulation during Heinrich events. Paleoceanography 20, PA2019.

Simon, Q., Bourlès, D. L., Bassinot, F., Nomade, S., Marino, M., Ciaranfi, N, Girone, A., Maiorano, P., Thouveny, N., Choya, S., Dewil, F., Scao, V., Isguder, G. Blamart, D., ASTER Team, 2017. Authigenic $^{10}Be/^{9}Be$ ratio signature of the Matuyama–Brunhes boundary in the Montalbano Jonico marine succession. Earth Planet. Sci. Lett. 460, 255–267.

Skinner, L.C., Shackleton, N.J., 2005. An Atlantic lead over Pacific deep-water change across Termination I: implications for the application of the marine isotope stage stratigraphy, Quat. Sci. Rev. 24(6), 571–580.

Sprovieri, R., Di Stefano, E., Incarbona, A., Gargano, M.E., 2003. A high- resolution record of the last deglaciation in the Sicily Channel based on foraminifera and calcareous nannofossil quantitative distribution. Palaeogeogr. Palaeoclimatol. Palaeoecol. 202, 119–142.

Suganuma, Y., Haneda, Y., Kameo, K., Kubota, Y., Hayashi, H., Itaki, T., Okuda, M., Head, M.J., Sugaya, M., Nakzato, H., Igarashi, A., Shikoku, K., Hongo, M., Watan-abe, M., Satoguchi, Y., Takeshita, Y., Nishida, N., Izumi, K., Kawamura, K., Kawa-mata, M., Okuno, J., Yoshida, T., Ogitsu, I., Yabusaki, H., Okada, M., 2018. Paleo-climatic and paleoceanographic records of Marine Isotope Stage 19 at the Chiba composite section, central Japan: a reference for the Early-Middle Pleisotocene boundary. Quat. Sci. Rev. 191, 406–430.

Sumner, G., Homar, V., Ramis, C., 2001. Precipitation seasonality in Eastern and Southern coastal Spain. International Journal of Climatology 21, 219–247.

Svenning, J.-C., 2003. Deterministic Plio-Pleistocene extinctions in the European cool-temperate tree flora. Ecol. Lett. 6, 646–653.

Till, C., Guiot, J., 1990. Reconstruction of precipitation in Morocco since 1100 AD based on *Cedrus* atlantica tree-ring widths. Quat. Res. 33(3), 337–351.

Trigo, R. M., Osborn, T. J., Corte-Real, J. M., 2002. The North Atlantic Oscillation influence on Europe: climate impacts and associated physical mechanisms. Climate research 20(1), 9-17.

Tolderlund, D.S., Bé, A.W.H., 1971. Seasonal distribution of planktonic foraminifera in the western North Atlantic. Micropaleontolology 17, 297–329.

Tzedakis, P. C., 2007. Seven ambiguities in the Mediterranean palaeoenvironmental narrative. Quat. Sci. Rev. 26(17-18), 2042–2066.

Tzedakis, P.C., Hooghiemstra, H., Pälike, H., 2006.The last 1.35 million years at Tenaghi Philippon: revised chronostratigraphy and long-term vegetation trends. Quat. Sci. Rev. 25, 3416–3430.

Tzedakis, P.C., Raynaud, D., McManus, J.F., Berger, A., Brovkin, V., Kiefer, T., 2009. Interglacial diversity. Nature Geoscience 2, 751–755.

Tzedakis, P.C., Channell, J.E.T., Hodell, D.A., Kleiven, H.F., Skinner, L.C., 2012a. Determining the natural length of the current interglacial. Nature Geoscience 5, 1–4.

Tzedakis, P. C., Wolff, E. W., Skinner, L. C., Brovkin, V., Hodell, D. A., McManus, J. F., Raynaud, D., 2012b. Can we predict the duration of an interglacial? Clim. Past 8, 1–13.

Vincent, E., Berger, W.H., 1981. Planktonic foraminifera and their use in Paleoceanography. In: Emiliani, C. (Ed.). The Oceanic Lithosphere. The sea vol. 7. John Wiley & Sons, New York, pp. 1025–1119.

Von Grafenstein, R., Zahn, R., Tiedemann, R., Murat, A., 1999. Planktonic $\delta^{18}O$ records at sites 976 and 977, Alboran Sea: stratigraphy, forcing, and paleoceanographic implications. In: Zahn, R., Comas, M.C., Klaus, A., et al. (Eds.). Proceeding of the Ocean Drilling Program, Scientific Results, College Station. TX, pp. 469-479. vol. 161, Ocean Drilling Program.

Waelbroeck, C., Labeyrie, L., Michel, E., Duplessy, J. C., McManus, J. F., Lambeck, K., Balbon, E., Labracherie, M., 2002. Sea-level and deep water temperature changes derived from benthic foraminifera isotopic records. Quat. Sci. Rev. 21(1-3), 295–305.

Wagner, B., Vogel, H., Francke F., Friedrich, T., Donders, T., Lacey, J., Leng, M., Regattieri, E., Sadori, L., Wilke, T., Zanchetta, G., Albrecht, C., Bertini, A., Combourieu-Nebout N., Cvetkoska, A., Giaccio, B., Grazhdani, A., Hauffe, T., Holtvoeth, J., Joannin, S., Jovanovska, E., Just, J., Kouli, K., Kousis, I., Koutsodendris, A., Krastel, S., Leicher N., Levkov, Z., Lindhorst, K., Masi, A., Melles, M., Mercuri, A.M., Nomade, S., Nowaczyk, N., Panagiotopoulos, K., Peyron, O., Reed, J.M., Sagnotti, L., Sinopoli, G., Stelbrink, B., Sulpizio, R., Timmermann, A., Tofilovska, S., Torri, P., Wagner-Cremer, F., Wonik, T., Zhang, X., 2019. Mediterranean winter rainfall in phase with African monsoon during past 1.36 million years. Nature 573, 256–260.

Walter, W., Harnickell, E., Mueller-Dombois, D., 1975. Climate Diagram Maps, Springer-Verlag.

Weaver, P.P.E., Pujol, C., 1988. History of the last deglaciation in the Alboran Sea (western Mediterranean) and adjacent North Atlantic as revealed by coccolith floras. Palaeogeogr. Palaeoclimatol. Palaeoecol. 64, 35–42.

Wennrich, V., Minyuk, P.S., Borkhodoev, V., Francke, A., Ritter, B., Nowaczyk, N.R., Sauerbrey, M.A., Brigham-Grette, J., Melles, M., 2014. Pliocene to Pleistocene climate and environmental history of Lake El'gygytgyn, Far East Russian Arctic, based on high-resolution inorganic geochemistry data. Clim. Past 10, 1381–1399. https://doi .org /10 .5194 /cp -10 -1381 -2014.

Yamasaki, M., Matsui, M., Shimada, C., Chiyonobu, S., Sato, T., 2008. Timing of shell size increase and decrease of the planktic foraminifer *Neogloboquadrina pachyderma* (sinistral) during the Pleistocene, IODP Exp. 303 Site U1304, the North Atlantic Ocean. Open Paleontology Journal 1, 18–23.

Yin, Q.Z., Berger, A., 2012. Individual contribution of insolation and CO_2 to the interglacial climates of the past 800,000 years. Climate Dynamics 38, 709–724.

Yin, Q.Z., Berger A., 2015. Interglacial analogues of the Holocene and its natural near future. Quat. Sci. Rev. 120, 28–46.

Ziveri, P., Thunell, R. C., Rio, D., 1995. Export production of coccolithophores in an upwelling region: Results from San Pedro Basin, Southern California Borderlands. Marine Micropaleontology 24, 335–358.

Ziveri, P., Baumann, K.-H., Boeckel, B., Bollmann, Young, J., Young, Y.R., 2004. Biogeography of selected Holocene coccoliths in the Atlantic Ocean. In: Thierstein, H.R. (Ed.), Coccolithophores: From Molecular Processes to Global Impact. Springer, Berlin, pp. 403–428.

Figure01

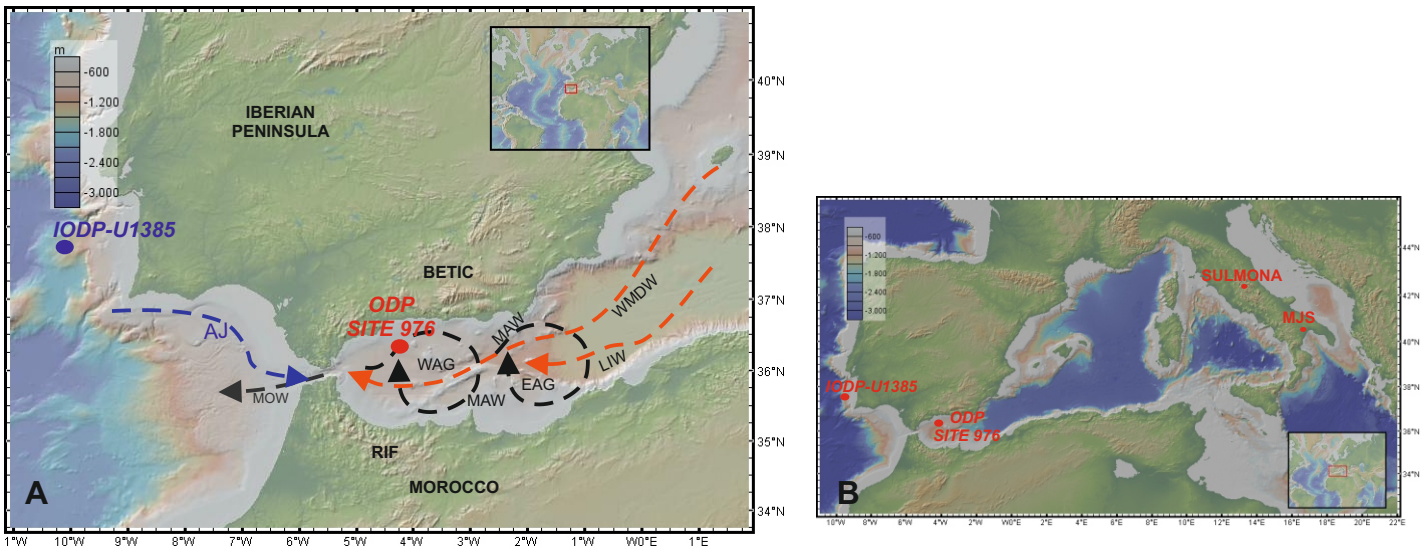
m
-600
-1.200
-1.800
-2.400
-3.000
IBERIAN
PENINSULA
IODP-U1385
BETIC
ODP
SITE 976
AJ
MOW
WAG
MAW
EAG
MAW
WMDW
LIW
RIF
MOROCCO
A
40°N
39°N
38°N
37°N
36°N
35°N
34°N
1°W
10°W
9°W
8°W
7°W
6°W
5°W
4°W
3°W
2°W
1°W
W0°E
1°E
SULMONA
MJS
IODP-U1385
ODP
SITE 976
B

Figure02

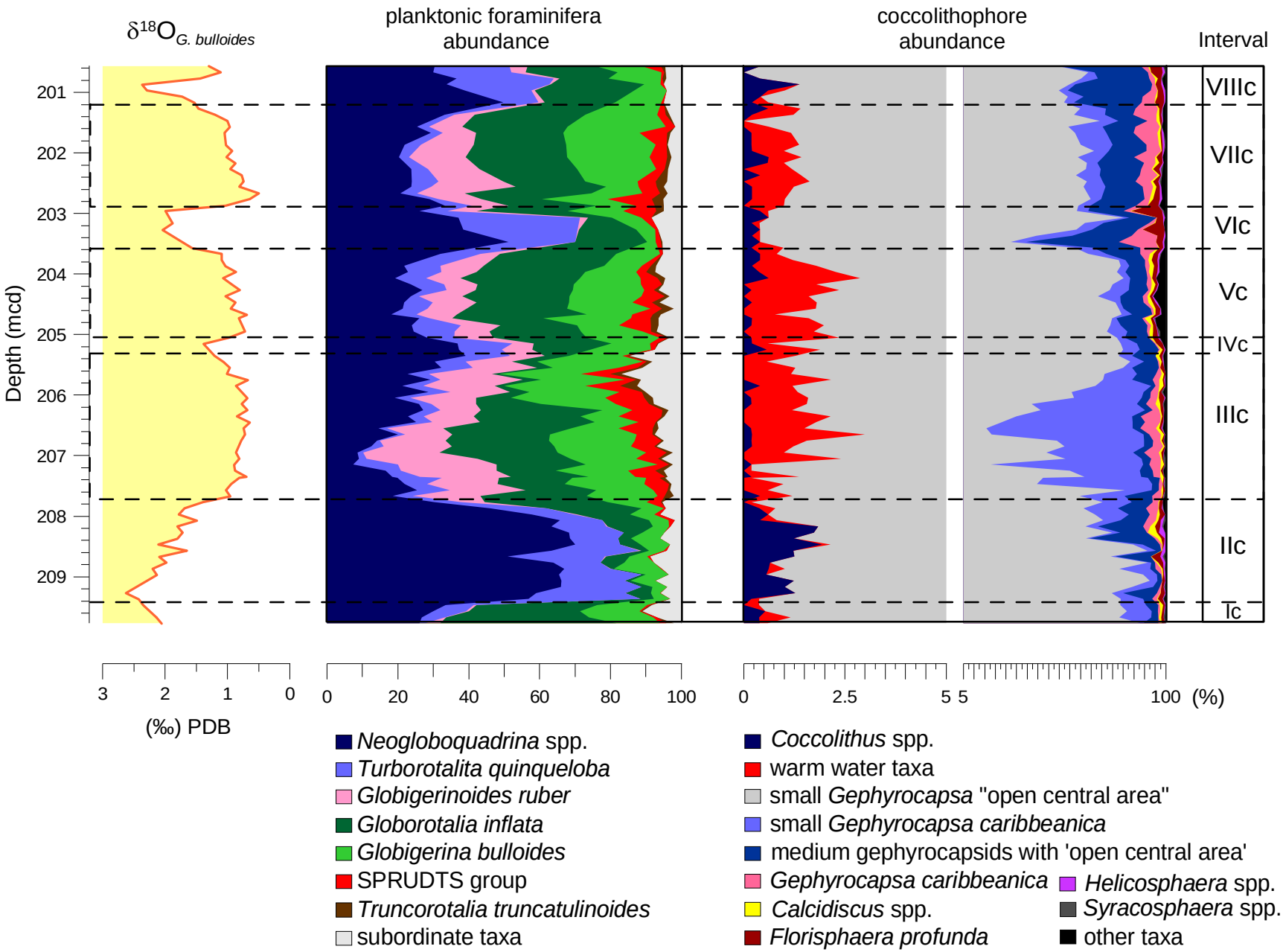
δ18OG. bulloides
planktonic foraminifera abundance
coccolithophore abundance
Interval
Depth (mcd)
201
202
203
204
205
206
207
208
209
VIIIc
VIIc
VIc
Vc
IVc
IIIc
IIc
Ic
3
2
1
0
(‰) PDB
0
20
40
60
80
100
0
2.5
5
5
100
(%)
Neogloboquadrina spp.
Turborotalita quinqueloba
Globigerinoides ruber
Globorotalia inflata
Globigerina bulloides
SPRUDTS group
Truncorotalia truncatulinoides
subordinate taxa
Coccolithus spp.
warm water taxa
small Gephyrocapsa "open central area"
small Gephyrocapsa caribbeanica
medium gephyrocapsids with 'open central area'
Gephyrocapsa caribbeanica
Calcidiscus spp.
Florisphaera profunda
Helicosphaera spp.
Syracosphaera spp.
other taxa

Figure03

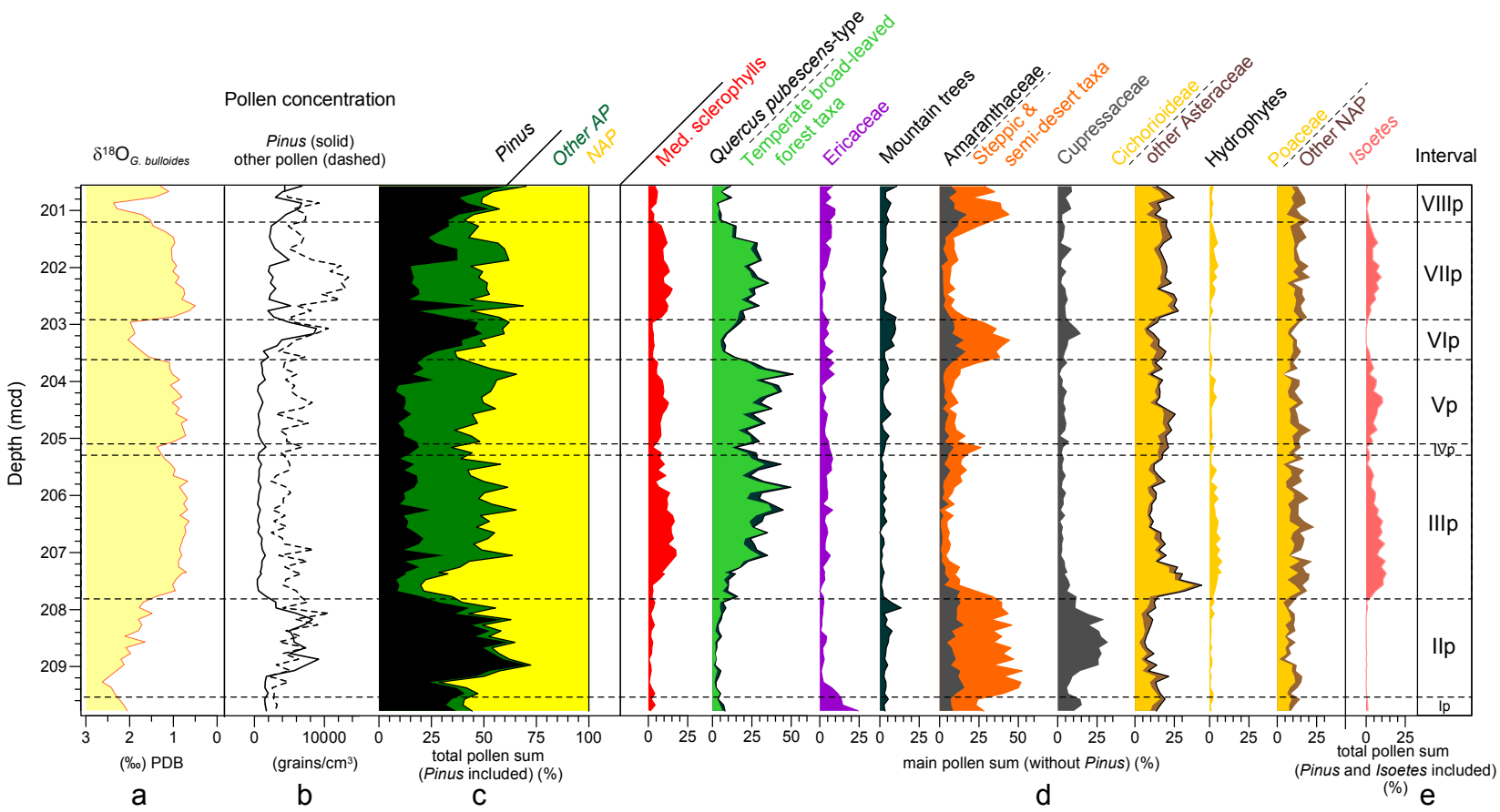
Pollen concentration
δ18O G. bulloides
Pinus (solid)
other pollen (dashed)
Pinus
Other AP
NAP
Med. sclerophylls
Quercus pubescens-type
Temperate broad-leaved forest taxa
Ericaceae
Mountain trees
Amaranthaceae
Steppic & semi-desert taxa
Cupressaceae
Cichorioideae
other Asteraceae
Hydrophytes
Poaceae
Other NAP
Isoetes
Interval
Depth (mcd)
201
202
203
204
205
206
207
208
209
VIIIp
VIIp
VIp
Vp
IVp
IIIp
IIp
Ip
3 2 1 0
(‰) PDB
a
0 10000
(grains/cm³)
b
0 25 50 75 100
total pollen sum
(Pinus included) (%)
c
0 25 0 25 50 0 25 0 25 0 25 0 25 0 25 0 25
main pollen sum (without Pinus) (%)
d
0 25
total pollen sum
(Pinus and Isoetes included)
(%)
e

Figure04

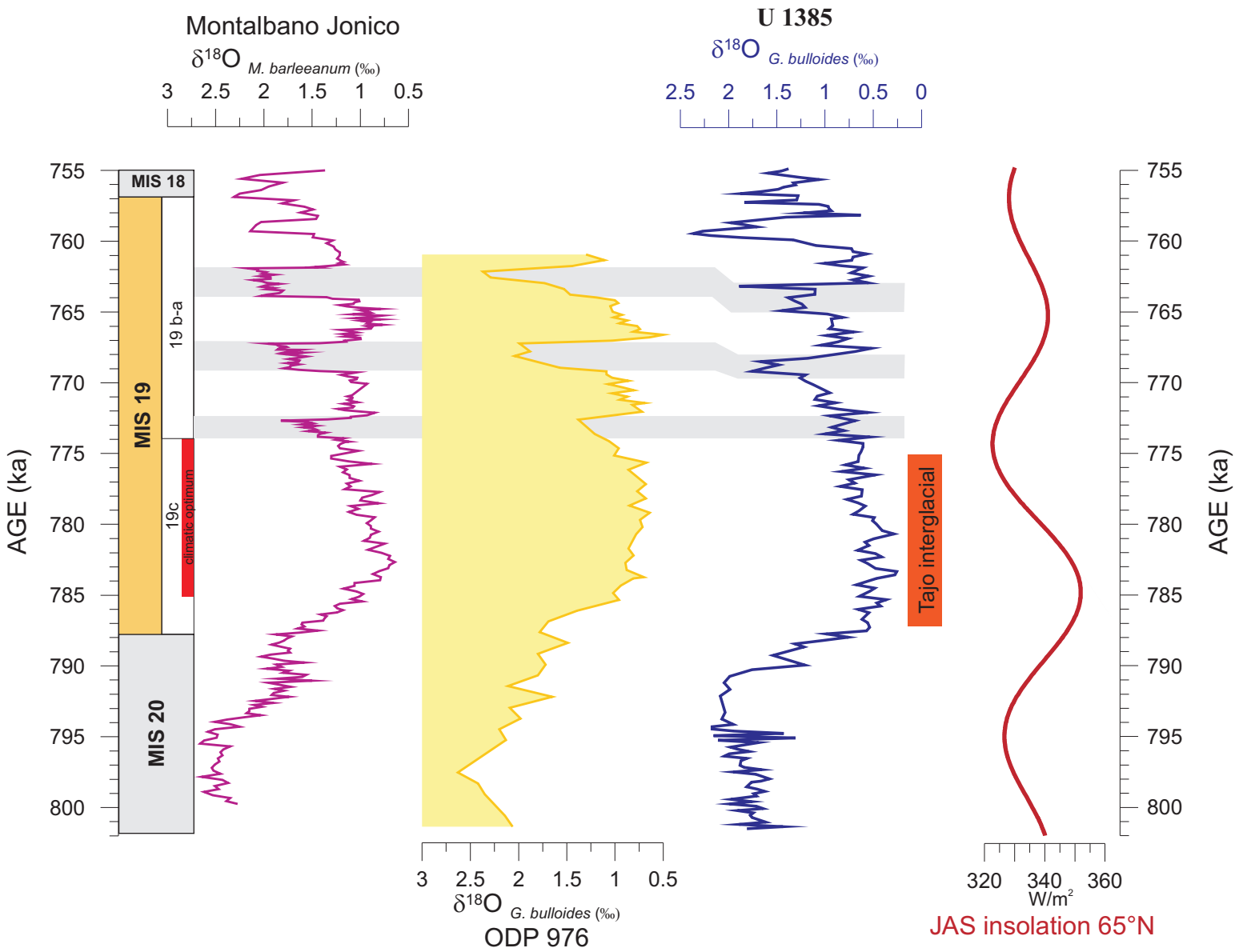
Montalbano Jonico
δ18O M. barleeanum (‰)
3 2.5 2 1.5 1 0.5
U 1385
δ18O G. bulloides (‰)
2.5 2 1.5 1 0.5 0
AGE (ka)
755 760 765 770 775 780 785 790 795 800
MIS 18
MIS 19
MIS 20
19 b-a
19c
climatic optimum
Tajo interglacial
3 2.5 2 1.5 1 0.5
δ18O G. bulloides (‰)
ODP 976
320 340 360
W/m2
JAS insolation 65°N

Figure05

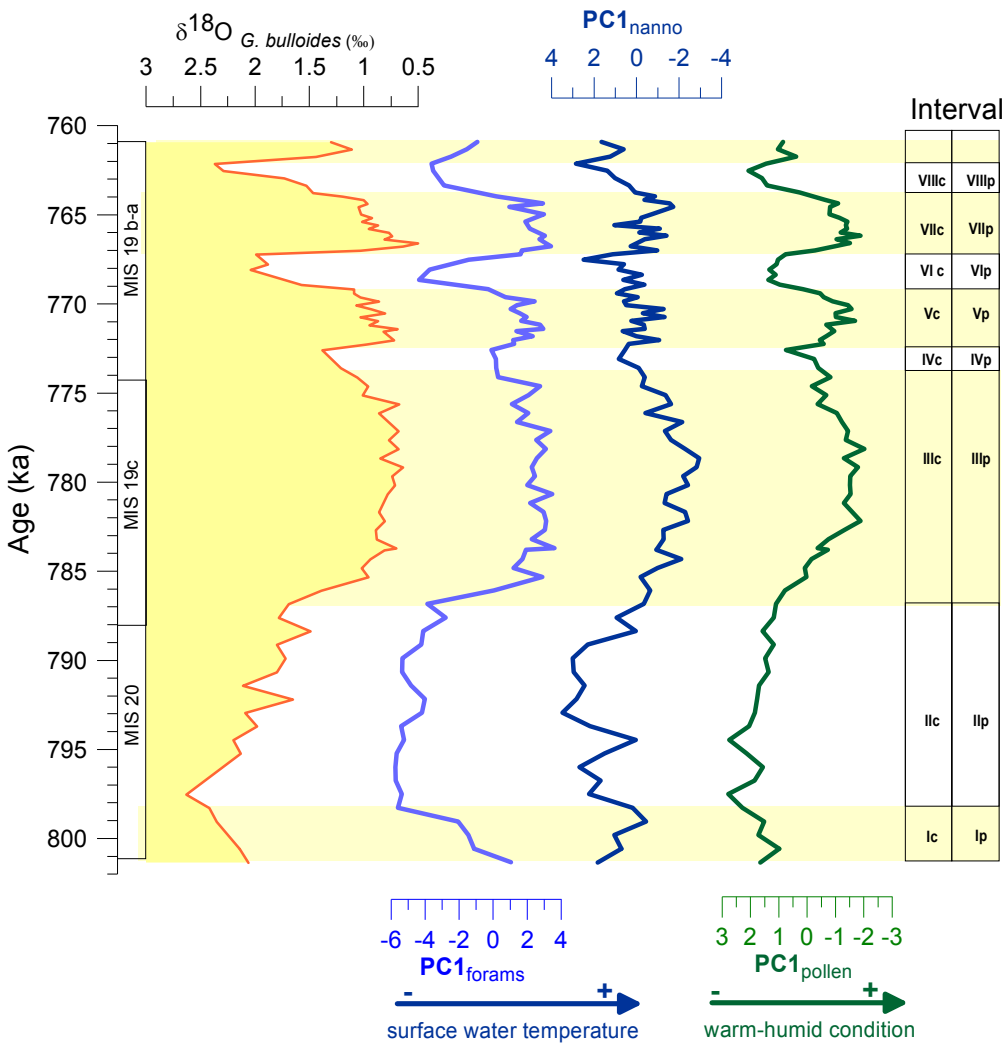
δ18O G. bulloides (‰)
3 2.5 2 1.5 1 0.5
PC1nanno
4 2 0 -2 -4
Interval
760
765
770
775
780
785
790
795
800
Age (ka)
MIS 19 b-a
MIS 19c
MIS 20
VIIIc VIIIp
VIIc VIIp
VI c VIp
Vc Vp
IVc IVp
IIIc IIIp
IIc IIp
Ic Ip
-6 -4 -2 0 2 4
PC1forams
-
+
surface water temperature
3 2 1 0 -1 -2 -3
PC1pollen
-
+
warm-humid condition

Figure06

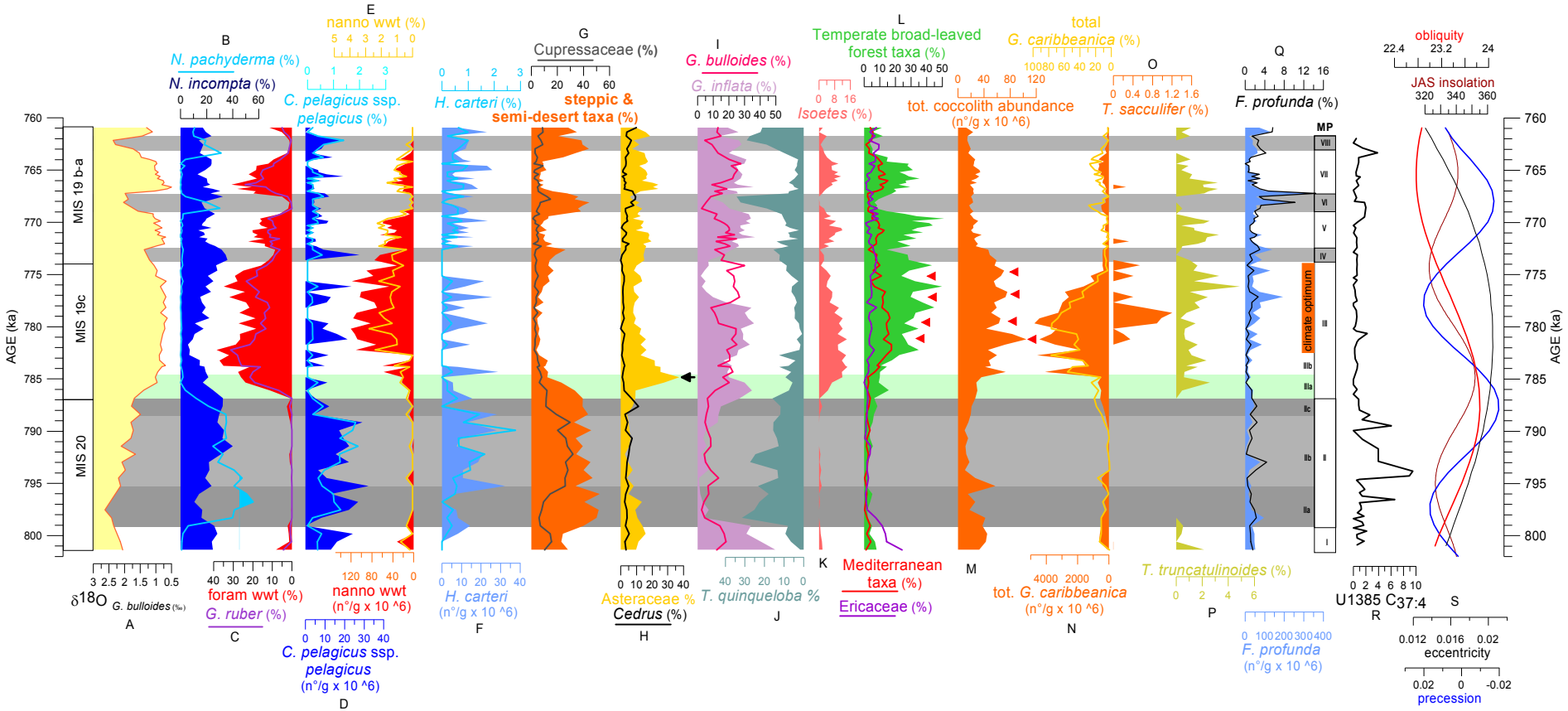
AGE (ka)
MIS 19 b-a
MIS 19c
MIS 20
δ18O G. bulloides (‰)
A
N. pachyderma (%)
N. incompta (%)
B
foram wwt (%)
G. ruber (%)
C
E
nanno wwt (%)
C. pelagicus ssp. pelagicus (%)
nanno wwt (n°/g x 10 ^6)
C. pelagicus ssp. pelagicus (n°/g x 10 ^6)
D
H. carteri (%)
H. carteri (n°/g x 10 ^6)
F
G
Cupressaceae (%)
steppic & semi-desert taxa (%)
Asteraceae % Cedrus (%)
H
I
G. bulloides (%)
G. inflata (%)
T. quinqueloba %
J
K
Isoetes (%)
L
Temperate broad-leaved forest taxa (%)
Mediterranean taxa (%)
Ericaceae (%)
M
total G. caribbeanica (%)
tot. coccolith abundance (n°/g x 10 ^6)
O
T. sacculifer (%)
tot. G. caribbeanica (n°/g x 10 ^6)
N
Q
F. profunda (%)
MP
climate optimum
T. truncatulinoides (%)
P
F. profunda (n°/g x 10 ^6)
obliquity
JAS insolation
U1385 C37:4
R
S
eccentricity
precession